B-spline based interval field decomposition method

Han Hu, Yi Wu, Anas Batou, Huajiang Ouyang

B-spline based interval field decomposition method

Han Hu[a,b], Yi Wu[b,c], Anas Batou[b,*], Huajiang Ouyang[a]

[a] *Department of Mechanical, Materials and Aerospace Engineering, School of Engineering, University of Liverpool, Liverpool L69 7ZF, United Kingdom*
[b] *MSME, Univ Gustave Eiffel, CNRS UMR 8208, Univ Paris Est Creteil, F-77474 Marne-la-Vallée, France*
[c] *State Key Laboratory of Advanced Design and Manufacturing for Vehicle Body, Hunan University, Changsha, 410082, China*

Abstract

In this paper, we contribute a new B-spline based interval field decomposition method as a non-probabilistic approach that takes into account local effects in interval field modelling. With B-spline basis functions, the interval field formulation is highly intuitive and easy to construct. The computational efficiency outperforms the traditional local interval field decomposition method. The explicit expression of the proposed method facilitates the use of optimisation methods in determining field bounds where deterministic local values are available. The proposed method can incorporate the use of truncated hierarchical B-spline basis functions and multi-patch stitching method that facilitate modelling of inhomogeneous interval fields, which effectively address the spatial variability of the parameters describing the interval field. A numerical case of a simply supported beam with non-deterministic material parameters subjected to external loads is performed to illustrate the applicability of the proposed method.

Keywords: Non-probablistic methods, interval field, B-spline, uncertainty quantification

1. Introduction

In practical engineering, non-deterministic approaches have become increasingly popular as a large range of real-world problems involve uncertainties. For example, heterogeneities properties of materials such as cement or biological tissues, varying external loads such as wind or snow loads, imperfections in geometries such as the dimensions of airframes of aircraft all involve a considerable level of uncertainties. These uncertainties are generally accounted for by two distinctive approaches, namely probabilistic and possibilistic methods. Probabilistic methods use the probability distributions of the uncertain parameters to propagate forwards the uncertainties and obtain the statistical properties of the quantities of interest. Among probabilistic methods, random fields [1, 2] are particularly suitable for modelling field uncertainties, in which the variability is spatially dependent. Moreover, the stochastic finite element method (SFEM) [3] was developed based on the random field concept for solving structural mechanics problems involving indeterminacy. However, the probabilistic methods require a massive amount of measurement data to estimate the probability

*Corresponding author
Email address: batoua@liverpool.ac.uk (Anas Batou)

distribution of the uncertain parameters, which is very expensive to obtain, or an assumed probabilistic distribution (often Gaussian), which demands expert knowledge and still requires some hyperparameters (indirect parameters, such as the correlation length) to be estimated.

On the other hand, possibilistic methods require less restrictive information about the uncertain variables and thus alleviate the need to identify a full probabilistic data description. The interval analysis method [4, 5] is a typical representative of this group as it specifies only the crisp bounds for the non-deterministic values. Fuzzy approach [6, 7] extends the interval method by introducing a membership function indicating to what extent a parameter belongs to a specific interval. Evidence theory [8, 9] and the imprecise probability method [10, 11] also belong to this group. Further information concerning these methods can be found in [12, 13]. Possibilistic methods are also extensively used in structural uncertainty analysis. For example, the interval finite element method (IFEM) [14, 15] was developed to obtain the structure's response bounds given the parametric input bounds. The main problem of IFEM (and other possibilistic methods mentioned above) is that it only concerns scalar uncertain variables such that each variable is deemed mutually independent. This mutual independence assumption brings two significant drawbacks in the presence of uncertain parameter field, namely expensive computational cost due to dimension explosion; and the loss of spatial dependency information resulting in unphysical realisations in practical engineering and an over-estimation of the output bounds. It was not until a decade ago that the concept of interval fields was proposed by Moens et al. [16] as an alternative to random fields in a non-probabilistic framework. In its original form, an interval field is represented by a linear combination of a series of independent interval factors multiplied with a set of deterministic basis functions. The spatial dependency is defined through these basis functions as they take the location-based vectors as input.

Over the past decade, research on the topic of interval field modelling has received much attention. Numerous interval field modelling methods have been developed and can be broadly categorised into the following three groups: explicit formulation, Karhunen-Loéve (K-L) expansion based formulation and convex descriptors based formulation [17]. The explicit formulation, to which the original form of the interval field method belongs, can be expressed as the superposition of spatially dependent basis functions, scaled by independent interval scalars as indicators of the magnitude of uncertainty. For the basis functions, Faes and Moens [18] proposed the Inverse Distance Weighting (IDW) interpolation method, where the basis functions interpolate the local uncertainty based on the inverse distance from several pre-defined control points to the rest of the field domain. The number and location of the control points depend on either the expert knowledge or indirect measurement data [19]. The major drawback of the IDW interpolation method is that the basis functions have non-vanishing values by definition throughout the whole domain, which hinders the expression of local effects. To address this issue, Mierlo et al. [20] proposed a scaled IDW interpolation method, in

which the standard IDW is adapted including an additional distance measure such that the weights can be manipulated in higher dimensional feature space to emphasise the local effects. Callens et al. [21] updated the weight function by locally supported quartic splines so that the basis functions have non-vanishing values only in an adjacent region around the control points and thus guarantee the local effects. Another set of basis functions is defined in the framework of the so-called Local interval field decomposition (LIFD) introduced by Imholz et al. [22, 23], where a set of piecewise second-order polynomial functions serve as basis functions with constraints on their bounds as well as maximum gradient as a measure of spatial dependency. Chen et al. [24] modified these basis functions into non-negative polynomials on their supports. However, the LIFD method has its limitations. Firstly, the restriction of the maximum gradient of the basis functions is not intuitive, as it is at most of the time not known *a priori*. Secondly, the intensive computational cost stands as a barrier for applying LIFD because the multiple evaluations of the polynomials can become cumbersome. Besides, the final form of the interval field formulation is not intuitive as the properties of the interval field, such as its interval centre and interval radius, can not be reflected directly from the formulation.

The K-L expansion based formulation for interval field modelling, proposed by Sofi [25], is an analogy to the random field generation stemming from the same theory with two significant modifications. First, the correlation function is replaced by the so-called spatial dependency function, which uses a midpoint operator of interval variables to quantify the spatial dependencies. Second, the concept of the extra unitary interval is introduced as the source of uncertainty, which is the corresponding counterpart of random variables in the K-L based random field formulation. Uncertainty propagation problems using such a formulation have been investigated towards Euler-Bernouilli beams [26, 25], Timoshenko beams [27] as well as large-scale realistic FE models [28]. The convex descriptors based formulation for interval filed (or process) modelling was firstly proposed by Jiang et al. [29]. In this formulation, the dependence between two points in the field is characterised by a convex model defined by the relevant angle and two ellipsoidal semi-axes. The convex model can be constructed by the available data [30] and was firstly aimed to deal with the time-variant and dynamic uncertainties [31] and then has been generalised to account for spatially varying uncertainties in structural mechanics [32]. Luo et al. [33] proposed the non-probabilistic series expansion (NPSE) method to model spatially varying uncertainties, the parameters of which are bounded by a multi-ellipsoid convex model. Recently, the NPSE method has been successfully applied in structural reliability assessment [34].

The present paper proposes a new explicit interval field formulation, termed B-spline Interval Field Decomposition (BIFD). In this formulation, the basis functions are a set of B-spline functions to account for spatial dependencies. By taking advantage of the partition of unity property of the B-spline functions, an intuitive form of the interval field that indicating the interval properties, such as interval centre and interval radius, can be trivially obtained. The computational cost is alleviated by using mature spline techniques,

which significantly improves the efficiency compared with the LIFD method, thus facilitating the BIFD method to be applied on higher-dimensional problems. Moreover, the problems of interval field construction with single and multiple deterministic local values are addressed, the bounds of which can be obtained through optimisation methods. Finally, as an extension to the BIFD method, an inhomogeneous interval field modelling method is provided, addressing the description of local effects with uniform or non-uniform interval properties.

The remainder of this paper is organised as follows. The BIFD method is introduced in Sec 2 with one-dimensional and multi-dimensional formulations. The quantification of an homogeneous interval filed with deterministic local values using BIFD method is addressed in Sec 3. For the extension of BIFD method to model inhomogeneous interval field, we propose to use truncated hierarchical B-spline basis functions and multi-patch stitching method, both of which are discussed in Sec 4. A numerical case is studied in Sec 5 of a simply supported beam subjected to uniformly distributed transversal loads, in which the Young's modulus and the cross-sectional diameter are modelled as interval fields. Finally, concluding remarks are given in Sec 6.

2. B-spline based interval field decomposition (BIFD) method

2.1. Interval analysis basics

The interval analysis and B-spline techniques serve as the foundations for the BIFD method and are thus provided in this section as preliminaries. A bounded uncertain parameter is an interval scalar X^{I}, which is a convex subset of the domain $\mathbb{R}$ constrained by its lower bound $\underline{X}$ and upper bound $\bar{X}$ as

$$X^{\mathrm{I}} = [\underline{X}, \bar{X}] = \{X \in \mathbb{R}, \underline{X} \leq X \leq \bar{X}\}. \tag{1}$$

The interval centre X_c and interval radius X_r are defined as

$$X_c = \frac{\underline{X} + \bar{X}}{2},\ X_r = \frac{\underline{X} - \bar{X}}{2}. \tag{2}$$

Similarly, an interval vector $\mathbf{X}^{\mathrm{I}} \in \mathbb{R}^{\mathrm{n}}$ is defined as a set of interval scalars as

$$\mathbf{X}^{\mathrm{I}} = \left\{ \begin{array}{c} X_1^{\mathrm{I}} \\ X_2^{\mathrm{I}} \\ \vdots \\ X_n^{\mathrm{I}} \end{array} \right\}. \tag{3}$$

The sample space of the interval vector $\mathbf{X}^{\mathrm{I}}$ is a multi-dimensional hypercube, in which the interval scalars are mutually independent, thus no dependency among the components are taken into account. For a deterministic function $\mathbf{Y} = f(\mathbf{X})$, which takes multidimensional input and generates multidimensional output, subjected to a vector $\mathbf{X}$ taken values from an interval vector $\mathbf{X}^{\mathrm{I}}$, the set formed by all outputs can also be seen as an interval vector such as

$$\mathbf{Y}^{\mathrm{I}} = \{\mathbf{Y} \in \mathbb{R}^{\mathrm{m}} \, | Y_i \in [\underline{Y}_i, \bar{Y}_i]\}, \tag{4}$$

where

$$\underline{Y}_i = \min_{\mathbf{X} \in \mathbf{X}^{\mathrm{I}}} f_i(\mathbf{X}),$$

$$\bar{Y}_i = \max_{\mathbf{X} \in \mathbf{X}^{\mathrm{I}}} f_i(\mathbf{X}),$$

where $f_i(\mathbf{X})$ denotes the i-th output generated by $f(\mathbf{X})$. The exact bounds for the output interval vector $\mathbf{Y}^{\mathrm{I}}$ are generally difficult to obtain and usually demand global optimisation methods [17]. However, the interval analysis often suffers from the over-conservatism that the interval radius of the output is usually larger than the *true* interval radius. Such a phenomenon is often termed 'dependency phenomenon' [35] and it stems directly from the neglection of dependencies among the input interval variables. The degree of over-conservatism is found to be related to the interval radii of the input/output interval variables as well as the dimensions of the problem [36]. Possible solutions to this problem are to consider the interdependency of the interval variables, e.g. by interval field modelling methods.

2.2. One-dimensional BIFD method

A general explicit formulation for interval field $\mathbf{\Phi}^{\mathrm{I}}(\mathbf{x}) : \tilde{\Omega} \times \mathbb{R}^{n_d} \mapsto \mathbb{R}$ is defined as

$$\mathbf{\Phi}^{\mathrm{I}}(\mathbf{x}) = \sum_{i=1}^{n_d} \psi_i(\mathbf{x}) \alpha_i^{\mathrm{I}}, \tag{5}$$

where $\psi_i(\mathbf{x}) : \tilde{\Omega} \mapsto [0, 1], \ i = 1, \ldots, n_d$ are basis functions representing the spatial uncertain patterns and $\alpha_i^{\mathrm{I}}, \ i = 1, \ldots, n_d$ are a set of independent interval scalars representing magnitude of uncertainty. In the IDW method, the basis functions are constructed based on the inverse of the distance to each predefined control point, and in the LIFD method, these are chosen as a set of piecewise second-order polynomial functions. In this paper, we propose to use B-spline functions as basis functions of the interval field. B-spline basis functions of degree k are built upon a non-decreasing knot vector $\Xi = \{t_1, t_2, ..., t_{N+k+1}\}$, where t_i is the i-th knot entry and N is the total number of the B-spline basis functions. A k-th degree univariate B-spline

basis function $B_{i,k}$ can be obtained recursively through the Cox-de Boor formula [37], such as for $k = 0$

$$B_{i,0}(x) = \begin{cases} 1 & t_i \leq x < t_{i+1} \\ 0 & \text{otherwise} \end{cases} . \tag{6}$$

and for $k > 0$

$$B_{i,k}(x) = \frac{x - t_i}{t_{i+k} - t_i} B_{i,k-1}(x) + \frac{t_{i+k+1} - x}{t_{i+k+1} - t_{i+1}} B_{i+1,k-1}(x) \ . \tag{7}$$

The B-spline basis functions possess a few merits that make them competitive over other choices:

- *Controllable continuity.* A k-th degree B-spline function is globally $\mathcal{C}^{k-1}$ continuous, which means that it has continuous derivatives up to order $k - 1$. The continuity can thus be manipulated by order elevation through (7).
- *Linear independence*, as they form a complete set of basis functions in the domain based on which they define.
- *Non-negativity.* All B-spline basis functions are non-negative on their support.
- *Partition of unity.* This property is vital for the interval field modelling and can be expressed as

$$\sum_{i=1}^{N} B_{i,k}(x) = 1, \ t_{k+1} \leq x \leq t_N. \tag{8}$$

For example, Fig.1 depicts a set of B-spline basis functions built on the knot vector $\hat{\Xi}_1 = \{0, 1, 2, \ldots, 10\}$

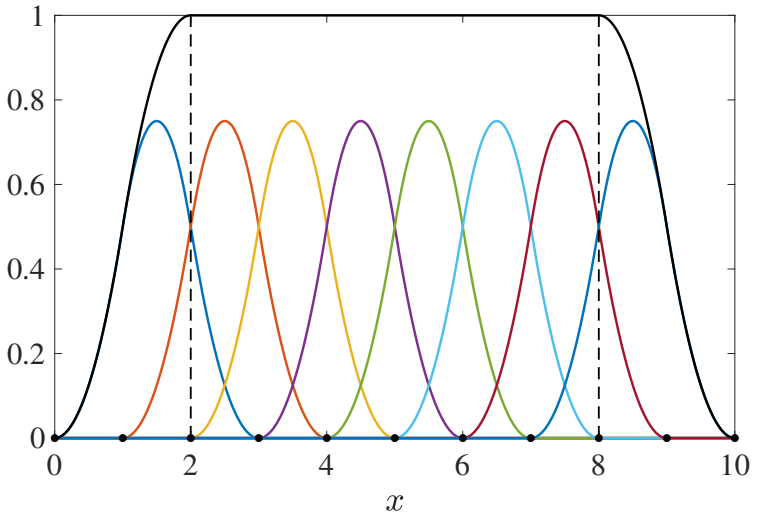

Fig. 1. Quadratic B-spline basis functions and their sum value.

(equispaced in [0, 10]) and their sum value. It can be observed that the sum value equals 1 when x takes

values from the third knot to the last third knot. Such a property is readily suitable for constructing a field with bounds.

Given the interval centre H_c and interval radius H_r, and an equispaced knot vector $\Xi = \{t_1, t_2, ..., t_{N+k+1}\}$ that encloses the domain of interest, an interval field formulation by BIFD method can be expressed intuitively with the use of $\{H_c, H_r\}$ as

$$\mathbb{H}^{\mathrm{I}}(x) = H_c + H_r \sum_{i=1}^{N} B_{i,k}(x)\, \xi_i^{\mathrm{I}},\ t_{k+1} \leq x \leq t_N, \tag{9}$$

where $B_{i,k},\ i = 1, \ldots, N$ are k-th degree B-spline basis functions defined on Ξ and $\xi_i^{\mathrm{I}} = \{\xi_i | -1 \leq \xi_i \leq 1\}\ i = 1, \ldots, N$ are unitary interval scalars that are called *interval field coordinates* (IFCs) in this paper. It is obvious that the field satisfies the prescribed bounds, such that $\mathbb{H}^{\mathrm{I}}(x) = [H_c - H_r,\ H_c + H_r]$. The extremities take place when all IFCs ξ_i^{I} take their upper/lower bound value, namely 1 or -1. The use of an equispaced knot vector guarantees that the B-spline basis functions are of the same shape, as shown in Fig.1, which is essential to model an homogeneous interval field.

The field domain of interest should be entirely enclosed by the set $[t_{k+1}, t_N]$ to validate the use of partition of unity. The authors note that in this setting, the total span of the knot vector is always larger than the field domain of interest. This oversize is due to abandoning the use of an *open knot* vector, in which the first and last knots are repeated $k+1$ times. B-spline basis functions defined on an open knot satisfies the partition of unity everywhere in the total span. However, this would cause some basis functions to deform and thus deviate heavily from others, especially at the edge of the domain. For example, Fig.2 shows a set of quadratic B-spline basis functions defined on an open knot $\hat{\Xi}_2 = \{2, 2, 2, 3, 4, 5, 6, 7, 8, 8, 8\}$. The sum of these functions satisfy the partition of unity everywhere in the domain spanned by the knot vector. However, the basis functions close to the edge are apparently distorted. Since only one basis function has a non-zero value at the edge, the realisation of this point in the field would depend solely on the interval scalar attached to that basis function, which means a loss of the information of spatial dependency.

To construct an interval field as (9), the next question is how to set the knot vector so that the spatial dependencies of points in the interval field can be incorporated into the basis functions. Considering $\Delta t = |t_i - t_{i+1}|,\ 1 \leq i \leq N + k$ as the knot span between two adjacent knots, a B-spline basis function of degree k typically has support over $(k+1)\Delta t$. The influence radius R_d [22] indicating the distance over which the B-spline basis function has a non-vanishing influence, can be defined as

$$R_d = (k+1)\Delta t/2. \tag{10}$$

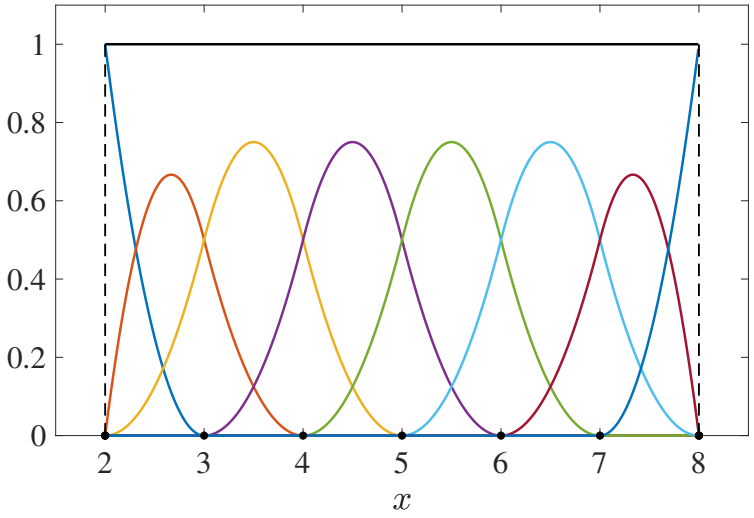

Fig. 2. Quadratic B-spline basis functions defined on an open knot vector and their sum.

Therefore, by predefining the influence radius R_d based on the knowledge of the spatial dependencies, the knot span can be readily derived.

This influence radius R_d can be compared with the commonly used 'correlation length' in the probabilistic approach. In Appendix A, the relation between these two parameters is investigated and a linear relation between them is found. Such an approximately linear relation implies that the influence radius of the interval field plays the role of the correlation length in the probabilistic framework.

The process for the generation of a 1D homogeneous interval field is summarised in Algorithm 1. To

Algorithm 1: 1D homogeneous interval field construction by BIFD

Input : Interval centre H_c, interval radius H_r, degree k.
(1) Determine the influence radius R_d and derive the knot span $\Delta t = 2R_d/(k+1)$.
(2) Extend $k\Delta t$ to the left side of the domain Ω, $|\Omega| = L$, and extend $(N+k)\Delta t - L$ to the right side of the domain, where $N = \text{ceil}(L/\Delta t)$.
(3) Discretise the extended field domain into $N + 2k$ elements with element size Δt and take all nodes to form the knot vector $\hat{\Xi}$.
(4) Build a set of B-spline basis functions of degree k with a total number N based on the knot vector Ξ.
(5) Generate realisations of $\{\xi_i\}_{i=1}^{N}$.
(6) Generate the interval field through (9).

illustrate the use of this algorithm, Fig.3 depicts four cases of interval fields with the same interval properties ($H_c = 0,\ H_r = 5$) and field domain $\Omega = [0, 10]$ but with different influence radius using BIFD method. Ten realisations are performed in each case. It can be observed that the influence radius indeed constrains the spatial dependencies among points as what a correlation length does in random fields modelling. Additionally, the authors note that the number of IFCs of the interval fields depends on the ratio of influence radius to the span of the field domain such that a small ratio results in a dense discretisation of the field domain and

thus a large number of IFCs. For the first case, this number is 32, while for the last case, only 4.

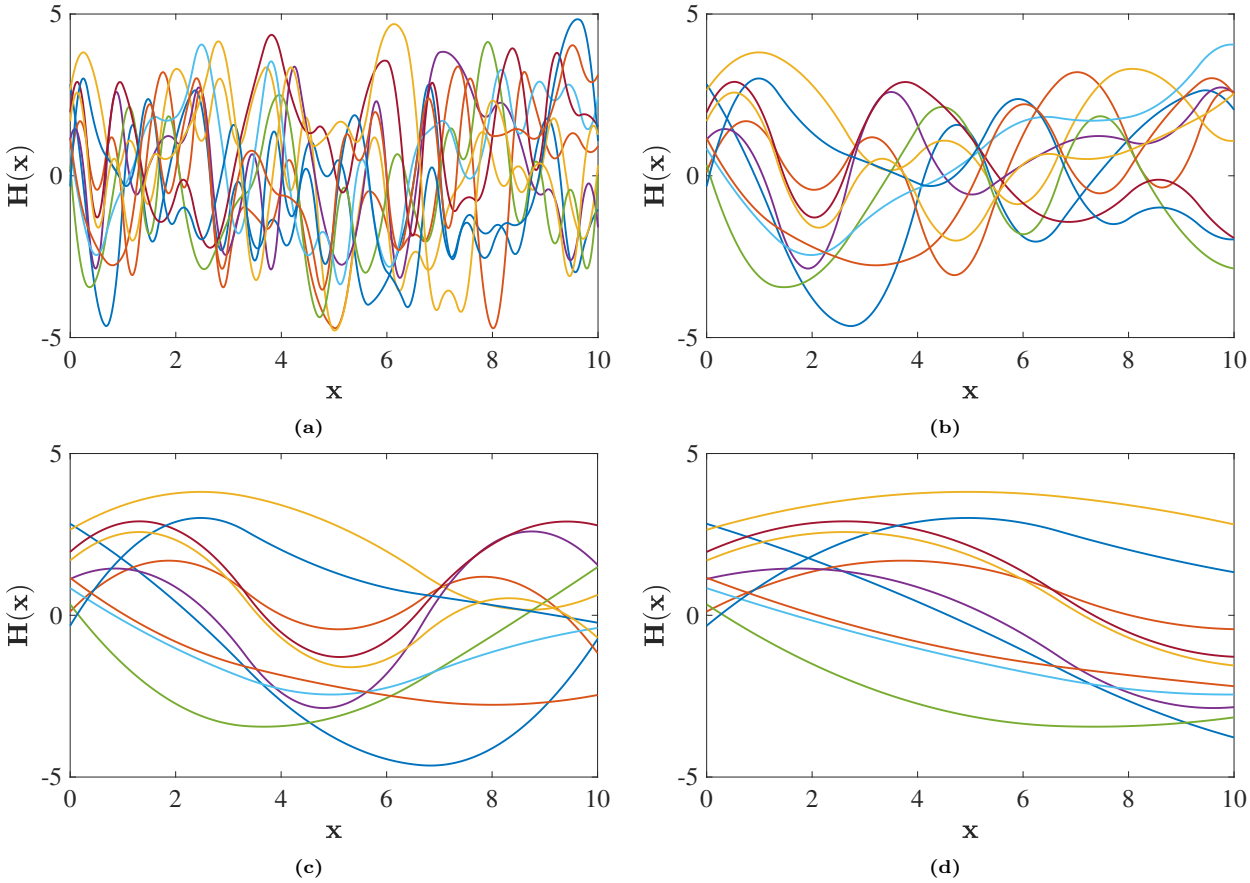

Fig. 3. 1D interval field realisations with influence radius equals to (a) 0.5; (b) 2.0; (c) 5.0; (d) 10.0.

2.3. Multi-dimensional BIFD method

The one-dimensional BIFD method can be readily extended to multiple dimensions by constructing the basis function as a tensor product of one-dimensional B-spline basis functions. Specifically, in two-dimensional case, the basis functions of degree k can be formed as

$$B^k_{i,j}(\mathbf{x}) = B_{i,k}(x)B_{j,k}(y), i = 1, \ldots, N_x,\ j = 1, \ldots, N_y, \tag{11}$$

and in three dimensions as

$$B^k_{i,j,l}(\mathbf{x}) = B_{i,k}(x)B_{j,k}(y)B_{l,k}(z), i = 1, \ldots, N_x,\ j = 1, \ldots, N_y,\ l = 1, \ldots, N_z, \tag{12}$$

where $\mathbf{x} = (x, y)$ in two-dimensional case and $\mathbf{x} = (x, y, z)$ in three-dimensional case, respectively. Hereafter, we restrict the discussion in two dimensions since the extension to three dimension is straightforward.

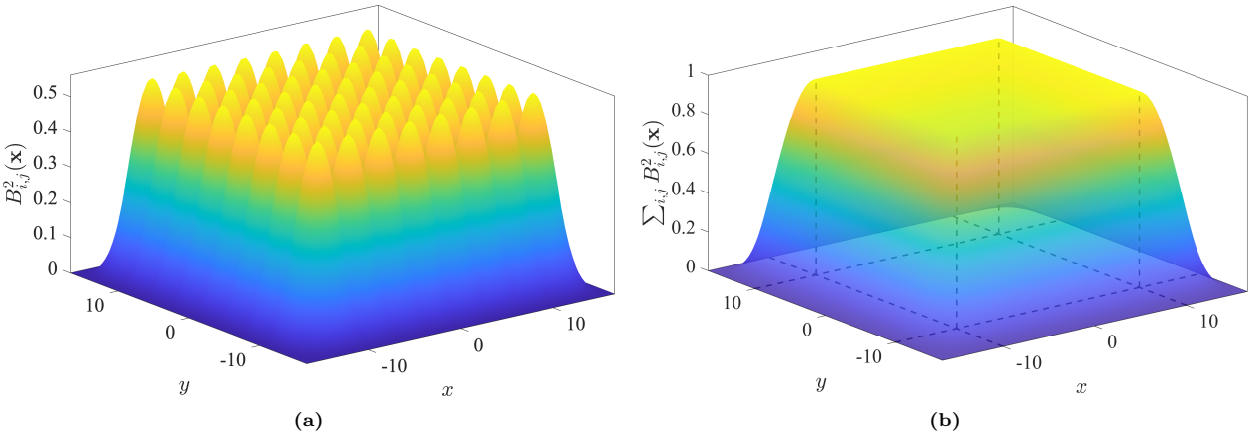

Fig. 4. (a) Basis functions in two-dimensional case; (b) partition of unity check in two dimensions.

The construction of knot vectors in x and y directions follows the same procedure in 1D case according to the field domain of interest in that dimension and can be done separately, such as $\Xi_x = [t_{x,1}, t_{x,2}, \ldots, t_{x,N_x+k+1}]$ and $\Xi_y = [t_{y,1}, t_{y,2}, \ldots, t_{y,N_y+k+1}]$. Afterwards, a set of B-spline basis functions $\{B_{i,k}(x)\}_{i=1}^{N_x}$ and $\{B_{j,k}(y)\}_{j=1}^{N_y}$ are built upon these knot vectors. The basis functions in two dimensions can thus be obtained through tensor product of these one-dimensional B-spline basis functions in x and y directions, as shown in (11). The partition of unity still holds in two dimensions, as

$$\sum_{i=1}^{N_x}\sum_{j=1}^{N_y} B^k_{i,j}(\mathbf{x}) = 1, \;\; t_{x,k+1} \leq x \leq t_{x,N}, \quad t_{y,k+1} \leq y \leq t_{y,N} \tag{13}$$

For example, the quadratic 2D basis functions for the field domain $\Omega^2 = [-10, 10] \times [-10, 10]$ with influence radius $R_d = 5$ in both directions is depicted in Fig.4a. The partition of unity holds that the sum of these basis functions equals 1 in the domain Ω^2, as shown in Fig.4b. Besides, the authors note that the knot vectors, the influence radius or even the degree of the B-spline basis functions are not necessarily confined to be the same in x and y directions. In fact, they can be set separately to form the 2D basis functions for a non-square field domain with different influence radii. Four 2D interval field realisations with different parametric settings are shown in Fig.5. The results show that the 2D-BIFD method can effectively model the interval field with a prescribed field domain of interest, influence radii in both dimensions, and interval properties.

Finally, the authors would like to note that the BIFD method also benefits from its high efficiency. Although dimension reduction is not involved in the interval field modelling with the BIFD method, the existing mature spline techniques facilitate the fast evaluation of B-spline basis functions and thus accelerate the construction of realisations. In Fig.6 the computational time between the LIFD method and the BIFD method are compared, where both methods are used to generate an interval field with the same resolution,

and a indicates the side length of the field domain. Both numerical experiments are performed on the MATLAB2021a platform with an Intel Core i9 (2.4GHz) CPU. It can be observed that as the growth of side length, the computational time required by the LIFD method increases to over 100s, while that by the BIFD method only increases slightly to less than 20s. The high efficiency of the BIFD method can facilitate its incorporation into a finite element (FE) model to solve complex solid mechanics problems.

Remark 1. *The authors would like to note that a large-scale FE problem does not necessarily involve a large number of interval variables leading to dimension explosion. This would only happen when the cross dependency of points in the field has a small influence radius, or many local refinements should be performed. However, we think such a problem exists universally in all interval field modelling methods: the smaller the cross dependency area covers and the more local information is incorporated, the more interval variables are needed, and thus, the more computational resource is required.*

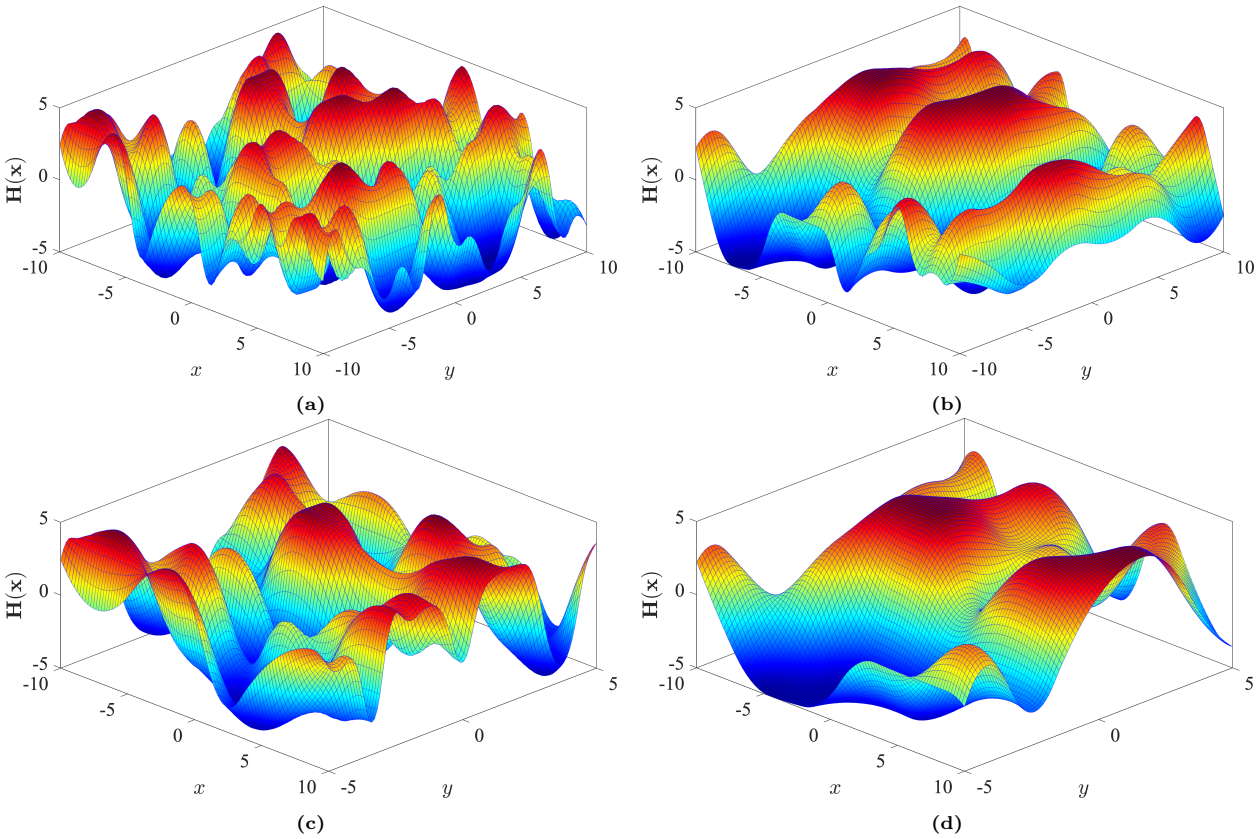

Fig. 5. 2D interval field realisations with $H_c = 0,\ H_r = 5$ and (a) $\Omega = [-10, 10]^2$ and $R_{dx} = R_{dy} = 2$; (b) $\Omega = [-10, 10]^2$ and $R_{dx} = 5,\ R_{dy} = 2$; (c) $\Omega = [-10, 10] \times [-5, 5]$ and $R_{dx} = R_{dy} = 2$; (d) $\Omega = [-10, 10] \times [-5, 5]$ and $R_{dx} = 5,\ R_{dy} = 2$.

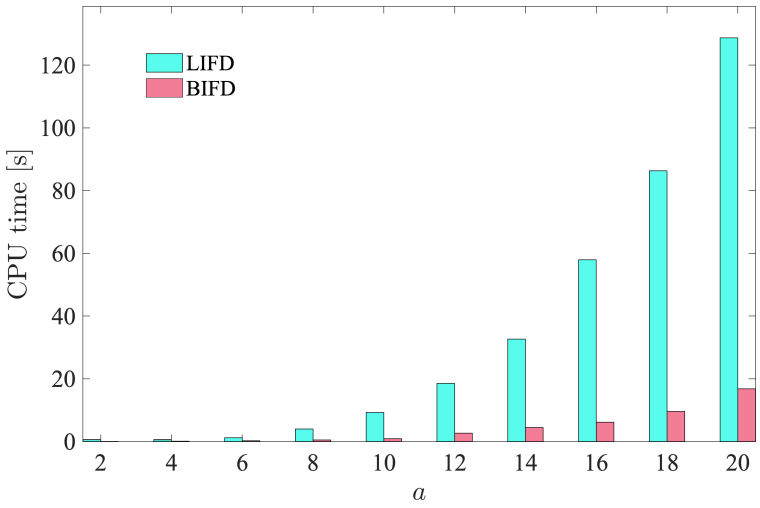

Fig. 6. Computational time comparison for LIFD and BIFD methods.

3. Interval field quantification with deterministic local values

In this section, the problem of constructing an interval field with some deterministic local values is addressed. These deterministic local values are given in the form that the values in certain locations of the field are fixed. The authors note that the field properties in this case are known *a priori* based on the expert knowledge. For those cases where the field properties are not known *a priori*, the problem becomes an identification problem, for which the parameters should be quantified beforehand [19, 38]. Uncertainty vanishes at these locations, which means all realisations of the interval field should pass through these points.

Let us start from a simple case where only a single deterministic local value is available. Suppose a one-dimensional domain Ω, on which an interval field is constructed with field properties $\{H_c, H_r, R_d\}$, has the value of the field at location x_o equal to h_o. The interval field can thus be expressed as

$$\mathbb{H}^{\mathrm{I}}(x) = H_c + H_r \sum_{i=1}^{N} B_{i,k}(x)\, \xi_i^{\mathrm{I}}, \tag{14}$$

where $\{B_{i,k}\}_{i=1}^{N}$ are k-th degree B-spline basis functions determined by Algorithm 1 and $\{\xi_i\}_{i=1}^{N}$ are independent IFCs. Considering the known local value, the following equation is established as

$$\mathbb{H}^{\mathrm{I}}(x_o) = H_c + H_r \sum_{i=1}^{N} B_{i,k}(x_o)\, \xi_i^{\mathrm{I}} = h_o. \tag{15}$$

For the B-spline basis functions of degree k, there are at most $k+1$ basis functions that take non-vanishing

values at a given point in the domain. The problem can thus be simplified as

$$\sum_{i=m}^{m+k} B_{i,k}(x_o)\,\xi_i^{\mathrm{I}} = \frac{1}{H_r}(h_o - H_c), \tag{16}$$

where $B_{i,k}(x_o)$ are non-vanishing B-spine basis functions for $i \in [m, m+k]$. To satisfy (16), unlike [22], the basis functions remain unchanged but the values of $\{\xi_i^{\mathrm{I}}\}_{i=m}^{m+k}$ are adjusted, and it will not yield the problem to the so-called 'maximum gradient' condition [22], because such a condition has already been satisfied implicitly by the determination of B-spline basis functions. It should be noted that in this case, $\{\xi_i^{\mathrm{I}}\}_{i=m}^{m+k}$ are not mutually independent anymore. Generally, the IFCs related to the $\max\{B_{i,k}(x_o)\}$ will be set as constraint interval variables, while others are set as free (but bounded) interval variables. Figure 7 shows several realisations of an interval field, in which all realisations cross the deterministic point $(0, 1)$.

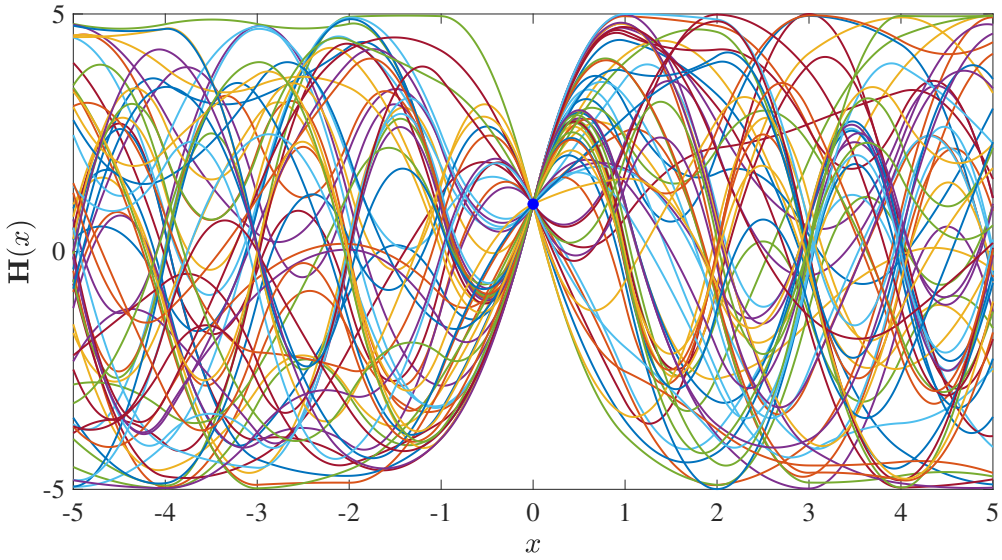

Fig. 7. Realisations of interval filed with $\Omega = [-5, 5]$, $H_c = 0$, $H_r = 5$, $R_d = 1.5$, $k = 2$ and the deterministic point locates at $(0, 1)$.

For the case with multiple deterministic local values, the interpolation method is similar but with additional complexity. With the same setting as the interval field properties mentioned in (15), suppose now a set of deterministic local values are given $\{(x_j, h_j)\}_{j=1}^{N_o}$ with $N_o \ll N$ and moreover those deterministic locations are spaced far enough from each other such that no $k+1$ points are located in the same knot span, which is set to ensure that the system is not over-constrained. Consider x_j is related to $k+1$ B-spline basis functions $\{B_{m,k}\}_{m=m_j}^{m_j+k}$, the constraints can be written in a matrix form as

$$\mathbf{A}\,\boldsymbol{\xi}^{\mathrm{I}} = \mathbf{b}, \tag{17}$$

where $\mathbf{A}$ is an $N_o \times N$ coefficient matrix containing B-spline basis functions evaluated at the deterministic locations, with notation $A(j, m_j : m_j + k) = [B_{m_j,k}, \ldots, B_{m_j+k,k}]$, $j = 1, \ldots, N_o$. The vector $\boldsymbol{\xi}^{\mathrm{I}} = \{\xi_1^{\mathrm{I}}, \ldots, \xi_N^{\mathrm{I}}\}^{\mathrm{T}}$ contains all IFCs and $\mathbf{b}$ is an $N_o \times 1$ right hand side vector with $b(j) = (h_j - H_c)/H_r$. Note that there will be $N - N_o$ IFCs to be set as free interval variables, and their values are used to determine those of the constrained ones.

The other quantities of interest are the changes of bounds of the interval field with some deterministic local values. It is reasonable to believe that those points in the vicinity of the deterministic locations have shrinking bounds due to the uncertainty reduction. Such constraints can also be used to impose boundary conditions to the field. The computation of the updated interval bounds of the field entails an optimisation method of the following problem, mathematically written as

$$\begin{aligned} &\text{Objective. } \min \mathbb{H}^{\mathrm{I}}(x) \text{ or } \max \mathbb{H}^{\mathrm{I}}(x), \ \forall x \in \Omega \\ &\text{s.t. } \mathbf{A}\,\boldsymbol{\xi}^{\mathrm{I}} = \mathbf{b} \\ &\xi_i^{\mathrm{I}} \in [-1, 1] \quad i = 1, \ldots, N. \end{aligned} \tag{18}$$

Finally, a numerical simulation is performed for an interval field with deterministic local values $\{(-4.0, -2.0)$, $(-2.0, -3.0)$, $(1.5, 4.0)$, $(3.5, 2.5)\}$ to illustrate the method. The interval field parameters are the same as the case shown in Fig.7. The results are presented in Fig.8(a), where the bold black line in the figure indicates the updated interval bounds obtained by optimisation method, e.g sequential quadratic programming (SQP) method [39]. The light lines enclosed by the interval bounds are Monte-Carlo realisations of the interval field. It is observed that the existence of the deterministic local values decrease the uncertain level in their proximity as expected and the interval bounds of those points are adjusted accordingly.

The interval field modelling with deterministic local values is much like training a Gaussian emulator [40], which is often used to infer the field uncertainty in a probabilistic regime when taking the deterministic local values as the training set. As a comparison, a Gaussian process emulator with the same deterministic local values is generated [41] as shown in Fig.8(b), where the solid line denotes the predicted mean value and the shaded area the predicted standard deviation. The emulator uses the radial basis function kernel with an inverse width $l_k = 1.5$ equivalent to the influence radius used in the interval field modelling. A few observations can be made as follows. (1) Given expert knowledge of the field properties and limited amount of measured information, both interval field and Gaussian emulator can be used to construct the uncertain model of the field with similar shapes; (2) For both models, the uncertainty decreases when the points are located in the vicinity of the deterministic locations, and the uncertainty level decreases to zeros at these

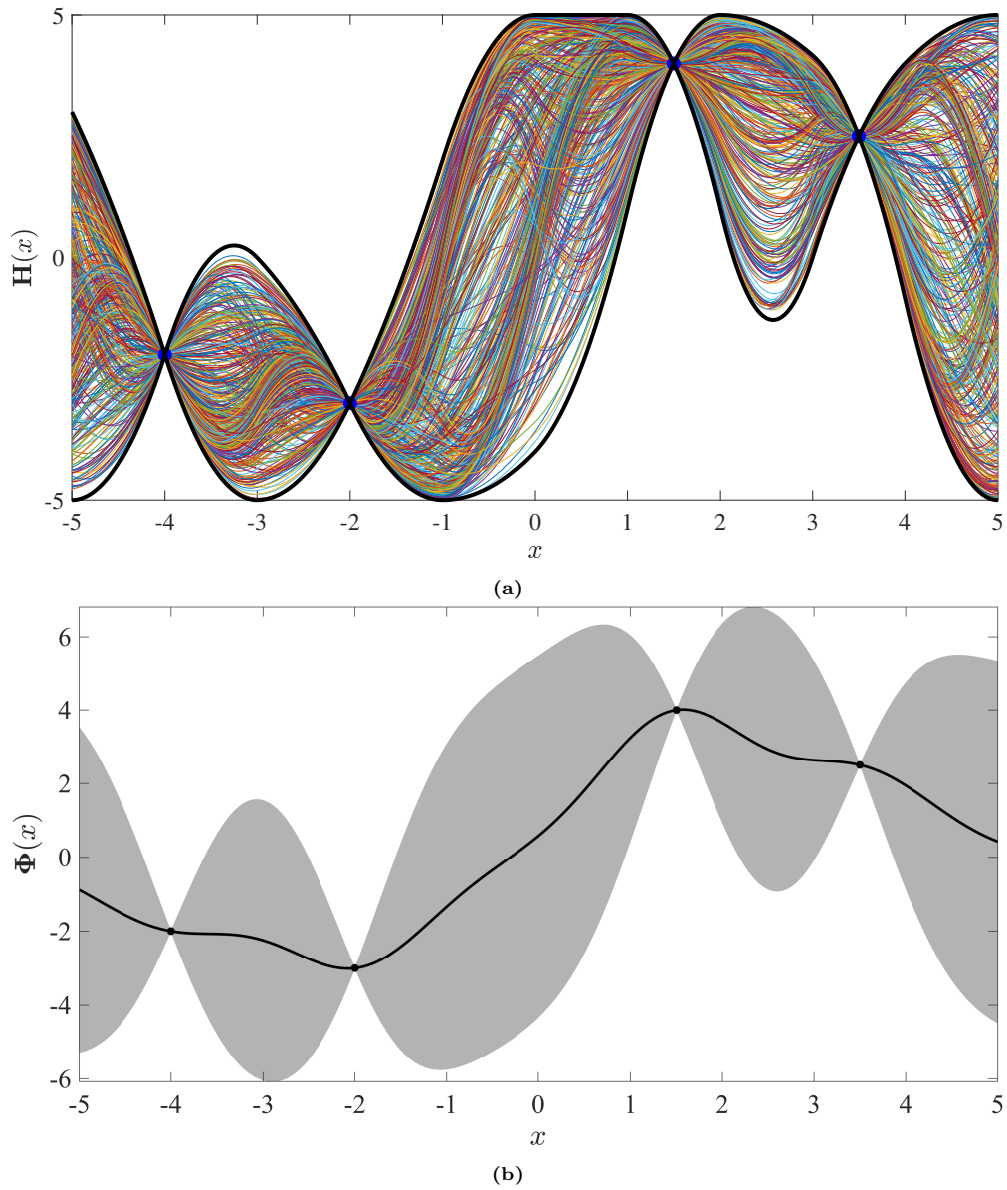

Fig. 8. (a) Interval field modelling with deterministic local values using BIFD method. Bold lines: the interval bounds, light lines: Monte-Carlo realisations; (b) Gaussian process emulator with deterministic local values as training set. Solid line: mean value, shaded area: standard deviation.

measured points; (3) The interval field model can compute the crisp bounds of every point in the field, while it can not determine the likelihood of the positions at which the points will be located. The Gaussian emulator, on the other side, is able to predict the confidence regions of the outputs but is not suitable to compute their bounds.

4. Inhomogeneous interval field modelling with BIFD

The proposed BIFD method is capable of modelling interval fields with spatially homogeneous interval properties such as interval centre and interval radius and spectral property such as influence radius. However, sometimes local effects in the field have to be taken into account, such as modelling local damage or spatial temperature variation, which requires locally variable interval and spectral properties. This section proposes two methods by modifying the original BIFD method, presented in previous sections, to account for local effects, which respectively use truncated hierarchical B-spline (THB-spline) basis functions and multi-patch stitching method. For illustration purposes, only one-dimensional case is discussed, but extensions to higher dimensions can be constructed following the same ideas with additional algorithmic complexity.

4.1. BIFD method with THB-spline basis functions

The B-spline basis functions can be locally refined by the use of hierarchical B-spline (HB-spline) basis functions [42]. To define the HB-spline basis functions, firstly a nested sequence of univariate B-spline function spaces of depth L

$$\mathcal{V}^0 \subset \mathcal{V}^1 \subset \cdots \subset \mathcal{V}^{L-1}, \tag{19}$$

are defined on the original domain Ω^0. Furthermore, a nested sequence of domains

$$\Omega^0 \supseteq \Omega^1 \supseteq \cdots \supseteq \Omega^{L-1}, \tag{20}$$

are used to define a hierarchical grid of depth L, where each domain Ω^l indicates the grid refined at level l. Each spline space $\mathcal{V}^l$ has a set of normalised basis functions $\mathcal{B}^l$ that spans the domain Ω^l. Following [43], the classical support definition is modified as

$$\text{supp} = \{\mathrm{x}|\ f(\mathrm{x}) \neq 0 \text{ and } \mathrm{x} \in \Omega^0\}, \tag{21}$$

and the HB-spline basis $\mathcal{H}$ can be constructed recursively as follows.

$$\begin{cases} \mathcal{H}^0 & := \{B^0 \in \mathcal{B}^0 \mid \text{supp } B^0 \neq \emptyset\} \\ \mathcal{H}^{l+1} & := \{B^l \in \mathcal{H}^l \mid \text{supp } B^l \not\subseteq \Omega^{l+1}\} \cup \{B^{l+1} \in \mathcal{B}^{l+1} \mid \text{supp } B^{l+1} \subseteq \Omega^{l+1}\}, \text{for } l = 0, \ldots, L-2. \\ \mathcal{H} & := \mathcal{H}^{L-1}. \end{cases} \tag{22}$$

The HB-spline functions essentially replace the basis functions of the lower level spline space ($\mathcal{V}^l$) by the basis functions of higher level spline space ($\mathcal{V}^{l+1}$) on the refined domain. This is feasible because those basis

functions of different levels are linearly dependent. As for a dyadic cell refinement, for which the cell size of adjacent level is related to a constant ratio of two, e.g. $h^l = 2h^{l+1}$, where h^l is the cell size of level l, such dependency can be explicitly represented as

$$B^l_{i,k}(\xi) = \sum_{r=0}^{k+1} \alpha^k_r \, B^{l+1}_{2i+r}(\xi), \;\; \alpha^k_r = \frac{1}{2^k} \binom{k+1}{r}, \tag{23}$$

where $B^l_{i,k}$ denotes the B-spline function of degree k on level l, α is the binomial coefficient. In this case, a B-spline function of degree k can be decomposed by $k+2$ B-spline functions defined on a dyadically refined cell. Dyadic cell refinement will be used throughout this section and an example of two adjacent levels of quadratic B-spline functions obtained by dyadic cell refinement is provided in Fig.9, where a quadratic B-spline function is decomposed into four higher level B-spline functions defined on the same domain. A typical way to construct HB-spline functions is indicated in Fig.10(a) and Fig.10(b), where a B-spline function of level 0 is replaced by four B-spline functions of level 1.

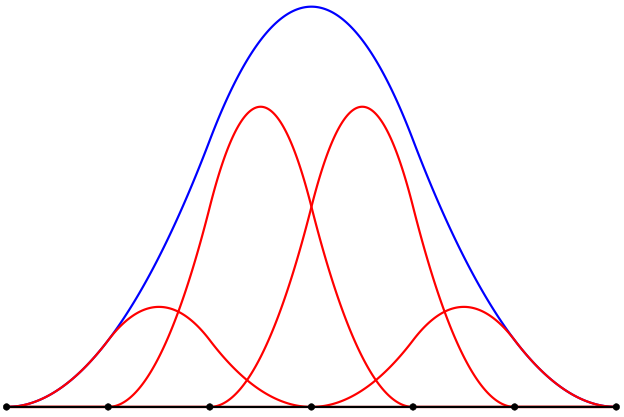

Fig. 9. Adjacent two levels of quadratic B-spline basis obtained by dyadic cell refinement.

However, HB-spline functions do not satisfy the partition of unity due to the overlapping of B-spline functions between adjacent hierarchical levels, which is not acceptable for the interval field modelling. On the other side, THB-spline functions fix this problem by truncating the B-spline functions of lower level in the overlapping region and thus preserve the partition of unity. Specifically, let B^l be a set of basis functions in $\mathcal{B}^l$ and according to (23), we can represent B^l with respect to the basis functions $B^{l+1} \in \mathcal{B}^{l+1}$ as

$$B^l = \sum c^{l+1}_{B^{l+1}}(B^l) \, B^{l+1}, \tag{24}$$

where $c^{l+1}_{B^{l+1}}(B^l) \in \mathbb{R}$ are coordination coefficients. The truncation of B^l concerning $\mathcal{B}^{l+1}$ in Ω^{l+1} is defined

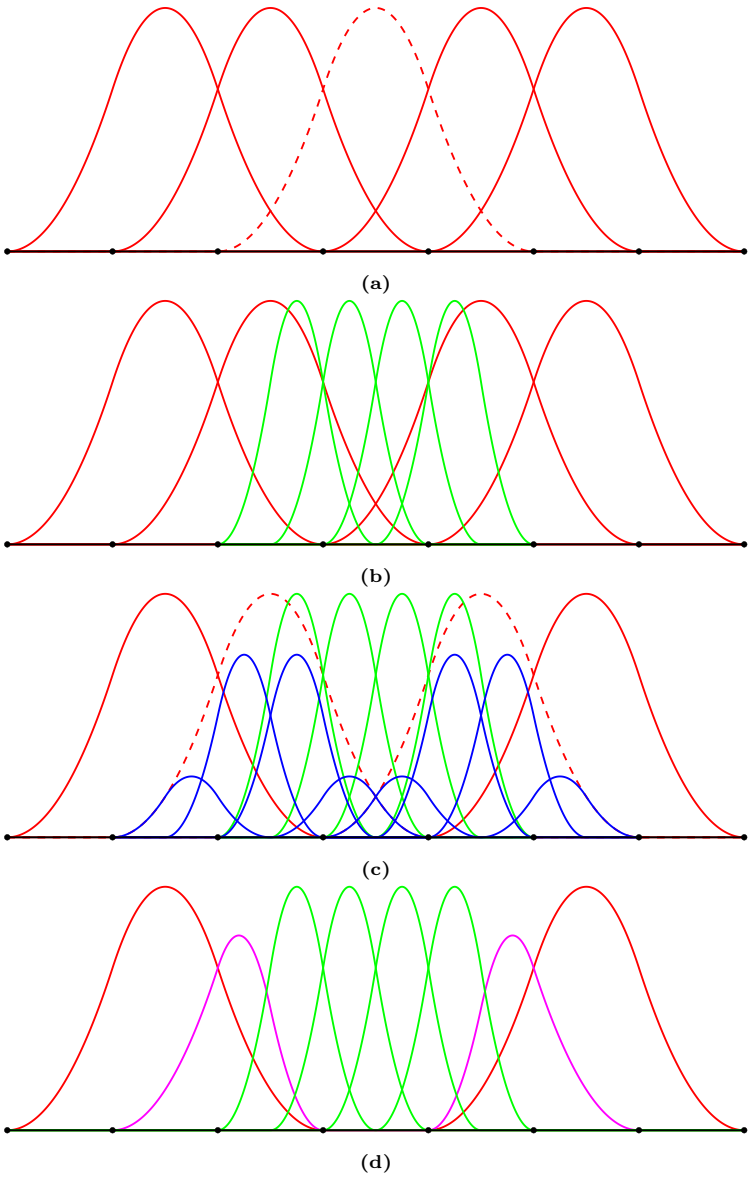

Fig. 10. The procedures to construct THB-spline basis functions. Red line: B-spline basis functions of level 0; green line: B-spline basis functions of level 1; blue line: decomposed B-spline components of level 1; purple line: truncated B-spline basis functions of level 0; dashed line: the B-spline basis functions to be replaced.

as

$$\text{trunc}^{l+1} B^l = \sum_{\text{supp } B^{l+1} \not\subset \Omega^{l+1}} c^{l+1}_{B^{l+1}}(B^l)\, B^{l+1}. \tag{25}$$

The THB-spline basis functions $\mathcal{T}$ can thereby be constructed recursively as

$$\begin{cases} \mathcal{T}^0 & := \mathcal{H}^0 \\ \mathcal{T}^{l+1} & := \{\text{trunc}^{l+1} \hat{B}^l | \text{ supp } \hat{B}^l \not\subseteq \Omega^{l+1}\} \cup \mathcal{H}^{l+1}, \text{for } l = 0, \ldots, L-2. \\ \mathcal{T} & := \mathcal{T}^{L-1}, \end{cases} \tag{26}$$

where the hat notation in $\hat{B}^l$ indicates the base could be truncated for multiple times and should be updated according to the most current state. The procedures to construct THB-spline functions from HB-spline functions are illustrated in Fig.10(c) and Fig.10(d), where two B-spline functions of level 0 overlapped with the B-spline functions of level 1 but not fully contained in Ω^1 are decomposed by the B-spline functions of level 1 as shown in Fig.9 and truncated by eliminating the components inside Ω^1.

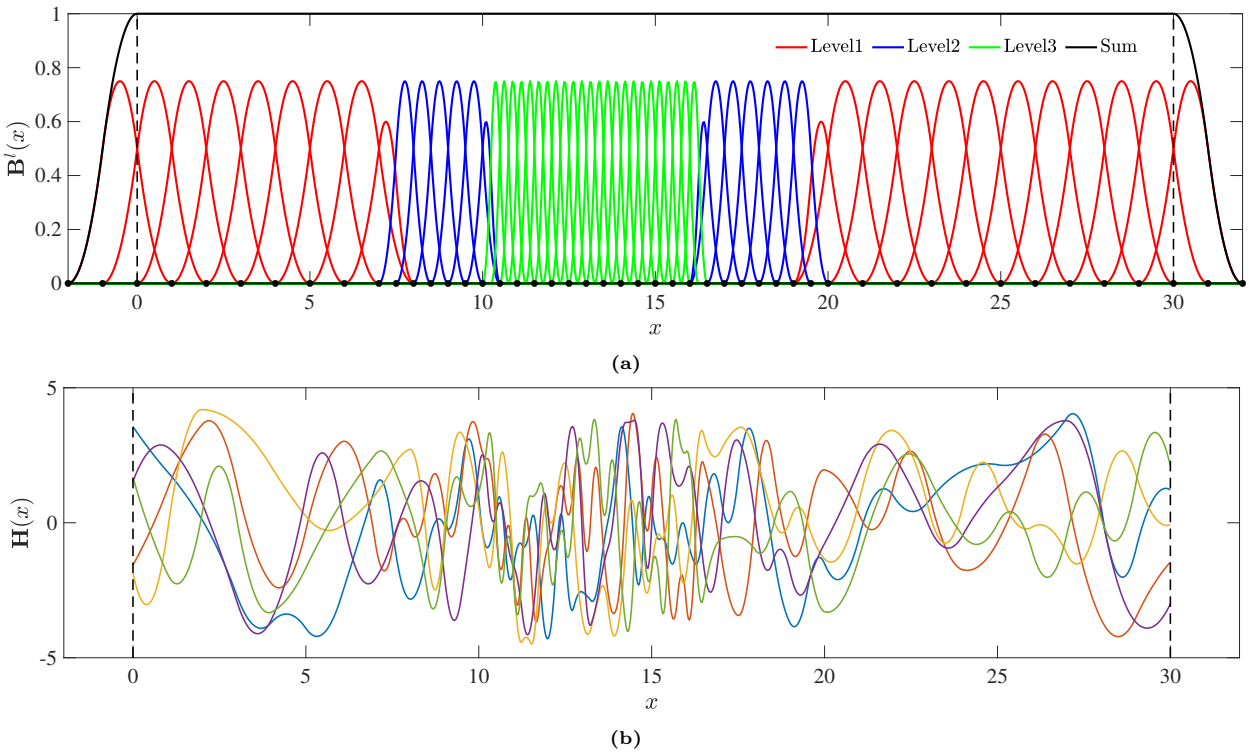

Fig. 11. (a) THB-spline basis functions with 3 hierarchical level and their sum; (b) interval fields modelling with THB-spline basis functions with $H_c = 0,\ H_r = 5,\ R_d^1 = 1.5,\ R_d^2 = 0.75,\ R_d^3 = 0.375$.

An inhomogeneous interval field can be constructed as follows. Suppose that the domain has the same interval properties (interval centre H_c and interval radius H_r) everywhere but a different spectral property (influence radius R_d) at certain areas. The THB-spline basis functions of degree k are built on knot vector $\Xi = \{t_1, t_2, \ldots, t_{N+k+1}\}$, which contains knots from all hierarchical levels up to depth L. Within each level N^l original B-spline basis functions and N_{tr}^l truncated B-spline basis functions are contained.The interval field can thus be represented as

$$\mathbb{H}^{\mathrm{I}}(x) = H_c + H_r \sum_{l=0}^{L-1} \sum_{i=1}^{N^l} B_{i,k}^l(x)\, \xi_{l,i}^{\mathrm{I}} + H_r \sum_{l=0}^{L-2} \sum_{j=1}^{N_{tr}^l} \hat{B}_{j,k}^l(x)\, \hat{\xi}_{l,j}^{\mathrm{I}},\ t_{k+1} \le x \le t_N, \tag{27}$$

where $\{B_{i,k}^l\}$ and $\{\hat{B}_{j,k}^l\}$ are the original and truncated B-spline basis functions of level l, respectively. $\{\xi_{l,i}^{\mathrm{I}}\}$ and $\{\hat{\xi}_{l,j}^{\mathrm{I}}\}$ are IFCs with bounds $[-1, 1]$. A numerical case is exemplified in Fig.11, where the interval field

realisations are constructed using 3-level THB-spline basis functions. The local effect can be observed within the support of B-spline basis functions of level 2 and level 3 in Fig.11(a) where the influence radius is only half and a quarter of that of level 0.

4.2. Multi-patch stitching method

BIFD method with THB-spline basis functions is suitable for modelling inhomogeneous interval fields with different local spectral properties, e.g. influence radii, while the interval bounds must be the same. However, it is no longer suitable if the interval field has varying interval centres or interval radii, such as spatially varying temperature or varying constitutive relations [20]. To tackle such problems, this section proposes the multi-patch stitching method. The multi-patch stitching method connects multiple fields with different interval properties or spectra properties, meanwhile satisfying continuity constraints at the connecting interfaces.

Suppose that a sequence of N one-dimensional continuous domains $\{\Omega_1, \Omega_2, \ldots, \Omega_N\}$ is at hand, each of which only has one element in common with their adjacent domains located in the interface and is mutually exclusive with other domains such as $\Omega_i \cap \Omega_{i+1} = \{t_i\},\ \Omega_i \cap \Omega_j = \emptyset,\ j \neq \{i-1, i, i+1\}$. Upon each domain Ω_i the interval properties H_c^i and H_r^i and influence radius R_d^i are defined individually so that a set of B-spline basis functions of degree k, e.g. $\{B_{j,k}^i\}$, can be constructed according to Algorithm 1. A set of interval fields can be modelled as

$$\mathbb{H}_i^{\mathrm{I}}(x) = H_c^i + H_r^i \sum_{j=1}^{N_i} B_{j,k}^i(x)\, \xi_{i,j}^{\mathrm{I}},\ x \in \Omega_i,\ i = 1, 2, \ldots, N, \tag{28}$$

where N_i is the number of B-spline basis functions defined on Ω_i and $\{\xi^{\mathrm{I}_{i,j}}\}$ are IFCs with bounds $[-1, 1]$. In order to preserve the $\mathcal{C}^{k-1}$ continuity (originated from the use of B-spline basis functions) at the interfaces between adjacent domains, following constraints need to be satisfied as

$$\begin{cases} \mathbb{H}_i^{\mathrm{I}}(t_i) = \mathbb{H}_{i+1}^{\mathrm{I}}(t_i) \\ \mathbb{H}_i^{\mathrm{I}(1)}(t_i) = \mathbb{H}_{i+1}^{\mathrm{I}(1)}(t_i) \\ \vdots \\ \mathbb{H}_i^{\mathrm{I}(k-1)}(t_i) = \mathbb{H}_{i+1}^{\mathrm{I}(k-1)}(t_i) \end{cases},\ i = 1, 2, \ldots, N-1 \tag{29}$$

where the superscript (j) indicates the j-th derivative. Note that (29) actually enforces constraints on the value of IFCs related to the interfacial knot t_i. Since the number of B-spline basis functions in the support of a specific point in the domain Ω_i is $k+1$, an equal number of IFCs will be involved. In this case, one IFC will be set as a free variable due to the fact that (29) has only k constraints while others are constrained variables whose values are dependent on this free variable.

Table 1: Interval properties and spectra properties.

Index	Domain Ω	Interval centre H_c	Interval radius H_r	Influence radius R_d
1	$[0, 5]$	0	1.0	1.0
2	$[5, 10]$	0	5.0	0.2
3	$[10, 15]$	0	2.0	0.5
4	$[15, 20]$	0	5.0	1.0
5	$[20, 25]$	0	1.0	0.3

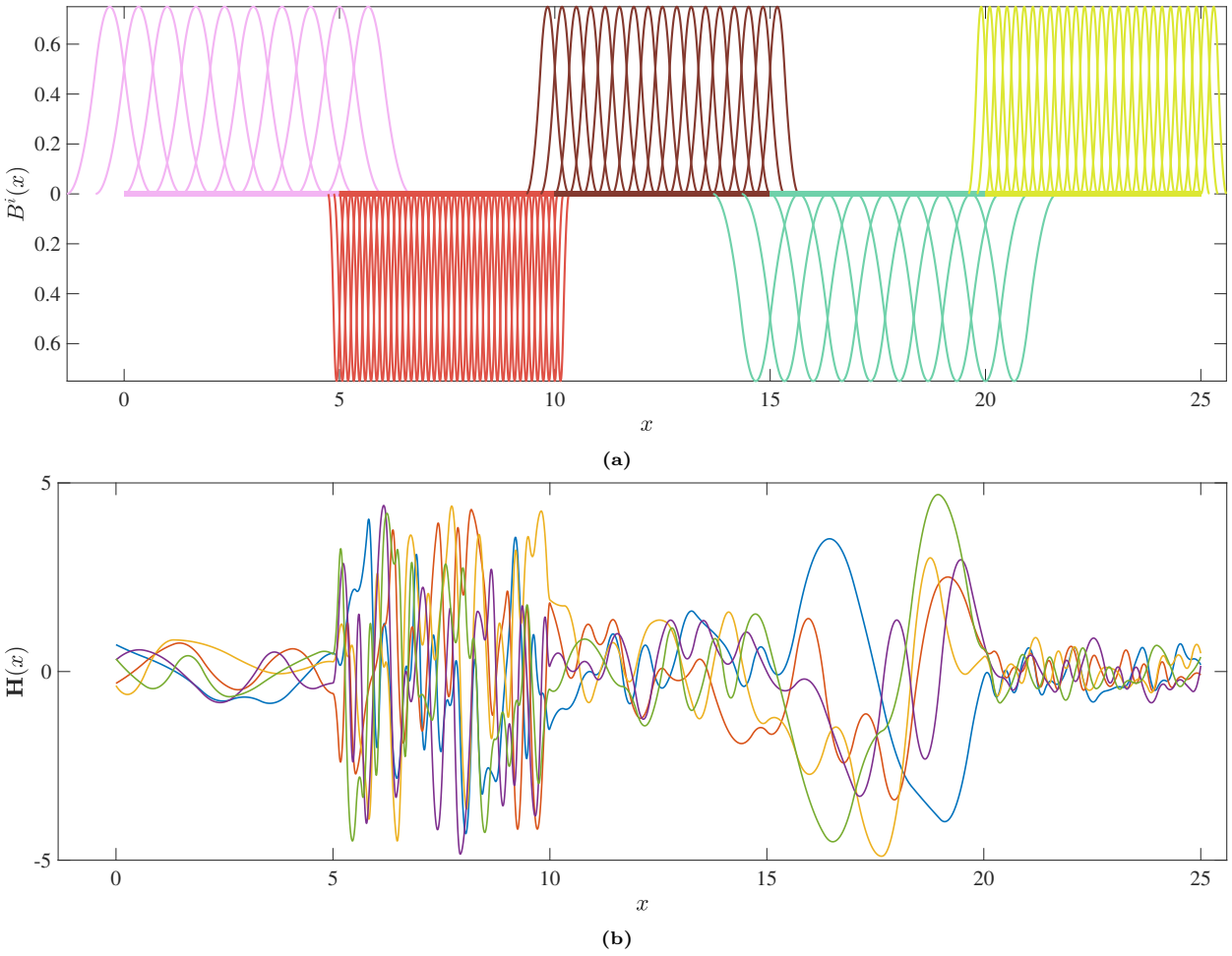

Fig. 12. (a) B-spline basis functions of five consecutive domains; (b) interval field realisations using multi-patch stitching method.

To illustrate the multi-patch stitching method, an example is provided that constitutes five consecutive interval fields with independent interval properties and spectra properties summarised in Table.1. The quadratic B-spline basis functions are built accordingly as shown in Fig.12(a), where the bold horizontal line with various colours indicates the domain in which the corresponding colour of B-spline basis functions are used to construct the interval fields. Finally, Fig.12(b) exhibits five interval field realisations modelling with these B-spline basis functions and field properties. It is observed that in each domain the realisations are

bounded by prescribed interval properties , and the local variations caused by imposing different influence radii also take effect as the realisations within $[5, 10]$ are significantly more fluctuant than that in $[15, 20]$. These results demonstrate that the multi-patch stitching method can effectively model inhomogeneous fields with locally defined field properties.

Remark 2. *The authors would like to note that the proposed methods to model inhomogeneous interval fields are not exclusive. Other methods may also be available to address local effects and varying internal radii. For instance, the use of a non-equispaced knot vector can model local effects, but it would result in the change of the whole knot vector, which has a global impact on the interval field. Multiplying the basis function of the interval field by a weight function can result in a local variation of the interval radius, but it can not change the interval centre. For conciseness, these methods are not further discussed in the present paper.*

5. Numerical application

In this section, two numerical cases are performed to illustrate the use of the BIFD method into solving structural mechanics problems. Specifically, a simply supported beam case and a steel plate case with some material parameters modelled as interval field are under investigation. These problems are solved using an interval finite element formulation, briefly described in Appendix B.

5.1. Case 1: Simply supported beam

A numerical case of a simply supported beam with non-deterministic material parameters is studied in this section to illustrate the incorporation of the proposed BIFD method. As shown in Fig.13, an Euler-Bernoulli beam of length L under simply supported boundary conditions at both ends, subjected to uniformly distributed transversal loads p_y, is discretised into 20 finite elements. The Young's modulus and the cross-sectional diameter are considered non-deterministic due to heterogeneities and manufacturing imperfections and are modelled as interval fields (termed as 'IF' model in the following content). The parameters used in the simulation are summarised into Table.2. The bounds of the first five order natural frequencies and the transverse displacement are investigated. As a comparison, the results of modelling the Young's modulus and the cross-sectional diameter as spatially independent interval variables (termed as 'II' model in the following content) and the results of modelling those parameters as single spatially constant interval variables (termed as 'SV' model in the following content) will also be presented. The output bounds are obtained by performing 10^5 Monte-Carlo realisations for all three non-deterministic models.

The results of the first five natural frequencies are shown in Fig.14(a), in which the bounds are represented by textured bars. The presented frequencies are normalised by the results of the deterministic model (termed

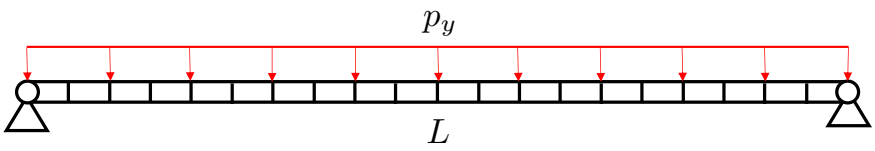

Fig. 13. Simply supported beam with uniformly distributed load.

Table 2: Simulation parameters for the numerical case.

Parameter	Density ρ [kg · m^{-3}]	Length L [m]	Loads p_y [N · m^{-1}]	Young's modulus E [GPa]	Influence radius R_{d_E} [m]	Cross-sectional diameter d_s [cm]	Influence radius R_{d_r} [m]
Value	7860	1	-500	[1.68, 2.52]	0.2	[8, 12]	0.5

as 'DM' model in the following content) of the corresponding order. The deterministic model takes the value of the interval centre of these non-deterministic parameters, such as Young's modulus $E_c = 2.1$ [GPa] and cross-sectional diameter $d_{sc} = 10$ [cm]. The results of the deterministic model can be obtained analytically [44] as

$$f_n = \frac{(n\pi)^2}{2\pi}\sqrt{\frac{E_c I_z}{\rho A L^4}},\ n = 1, 2, 3, \dots \tag{30}$$

where $I_z = \pi d_{sc}^4/64$ is the polar moment of inertia of the section and $A = \pi d_{sc}^2/4$ is the area of the section. It can be observed that for all presented five natural frequencies, the output bounds of the 'SV' model encloses those of the 'IF' model, which then encloses the output interval bounds of the 'II' model. These findings are supported by examining the bounds of the transversal displacements, as shown in Fig.14(b). The 'SV' model shows the least restrictive bounds for the transversal displacement, whereas the 'II' model shows the most restrictive ones. The output bounds of the 'IF' model lies in between, and the result of the 'DM' model is enclosed by all the output bounds of the above models. These results indicate that the 'SV' model, which can be seen as the 'IF' model with an infinitely large influence radius, always generates the broadest interval bounds for the output as it corresponds to a less informative model. On the other side, the 'II' model, which can be seen as the 'IF' model with an infinitely small influence radius, becomes too conservative as it ignores all the spatial dependency information. As a comparison, the 'IF' model takes the nondeterminency as well as the spatial dependency into account so as to generate reasonable output interval bounds without being too conservative.

Another point the authors would like to note is that the 'IF' model results can be totally different if some known local values are predefined in the field. For example, Fig.15 presents the results in which the 'IF' model contains two deterministic local values for the cross-sectional diameter, while other parameters stay unchanged (Fig.16 shows 100 realisations of the interval field of the cross-sectional diameter). It can be observed from Fig.15(a) that the bounds of the first five order of natural frequencies of the 'IF' model

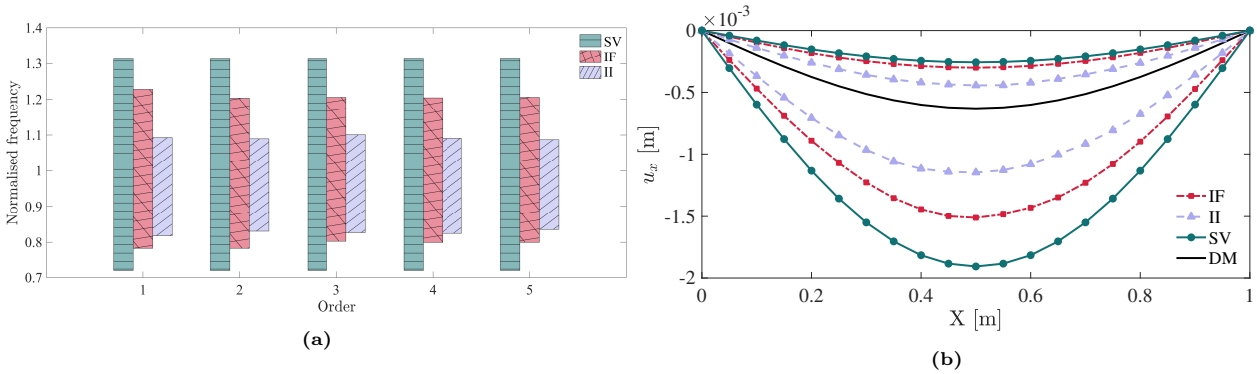

Fig. 14. (a) First five normalised natural frequencies; (b) the transversal displacements.

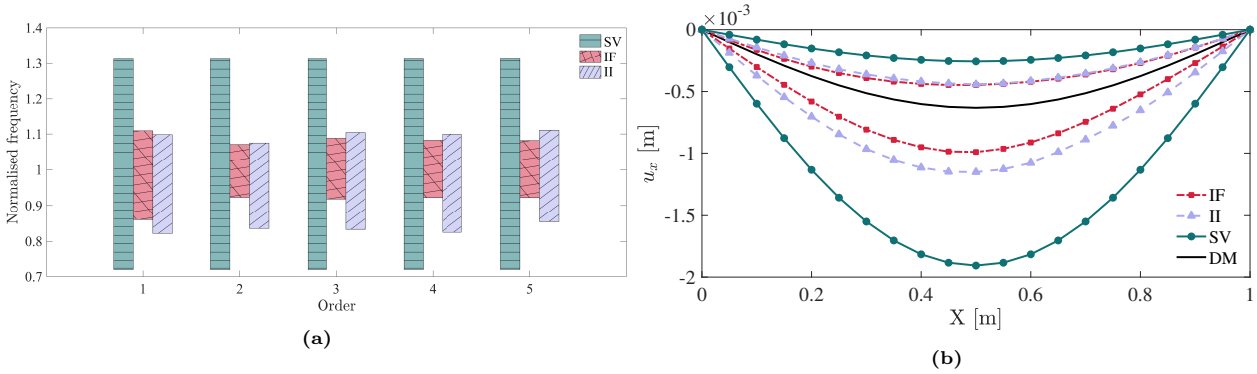

Fig. 15. (a) First five normalised natural frequencies and (b) the transversal displacements with known local values as $d_s(0.2250) = 9.5$ [cm] and $d_s(0.7250) = 10.5$ [cm].

substantially reduce compared with the case containing no known information. Moreover, except for the first order, the resulting bounds of natural frequencies of the 'IF' model are enclosed by those of the 'SV' model and the 'II' model. Similar results can be obtained considering the transversal displacement, as shown in Fig.15(b). The displacement bounds of the 'IF' model become the most restrictive compared with the 'SV' model and the 'II' model. These results indicate that the deterministic local values in the interval field can significantly reduce the uncertainties and thus reduce the range of the outputs' bounds.

5.2. Case 2: Steel plate

In this section, the plane-stress problem of a steel plate is presented to illustrate the incorporation of a 2D interval field modelled by BIFD method to solve a 2D problem. The problem setting is depicted in Fig.17(a), where the geometry can be considered as a square with a quarter of a circle in its left-bottom corner subtracted. The left edge of the plate is fixed and the motion in the y-direction of the bottom edge is constrained. A uniform external pressure is applied to the right edge of the plate. The thickness of the plate is taken as 1 [mm]. The linear elastic material is used with Poisson's ratio $\nu = 0.3$ and Young's modulus modelled as an interval field. The upper and lower bounds of the stress and displacements in the x-direction

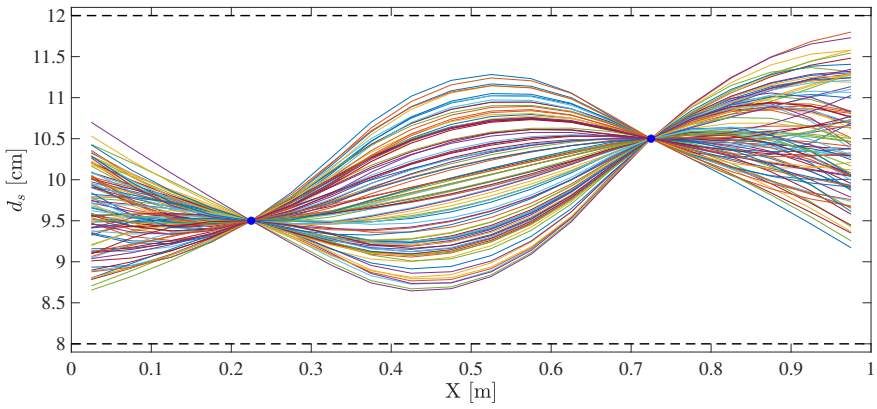

Fig. 16. A hundred realisations of cross-sectional diameter with two deterministic local values.

are of our interest. To solve such a problem, the plate is firstly discretised using structured quad mesh, as shown in Fig.17(b).

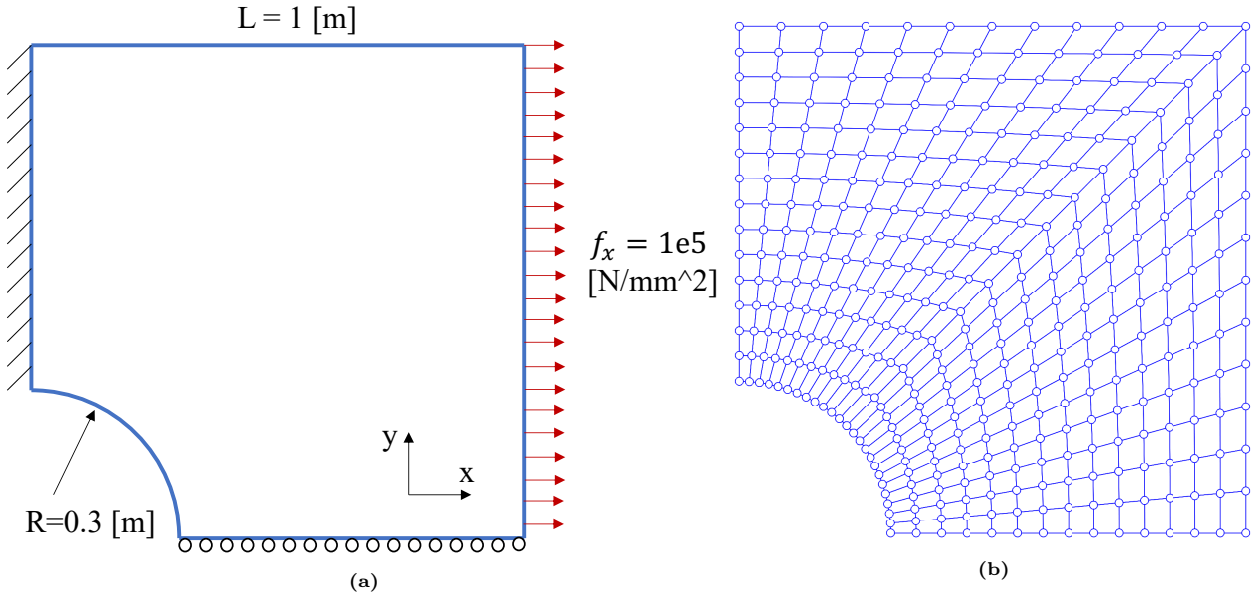

Fig. 17. (a) Problem setting for the steel plate; (b) adopted FE mesh.

The uncertain parameters for the interval field modelling Young's modulus are introduced as follows: the interval centre $E_c = 200$ [GPa] and interval radius $E_r = 20$ [GPa]. The influence radius is isotropically 0.5 [m] in the whole domain except for a refined part in the area $\{(x, y)|\ 0.5 \leq x \leq 1, 0.5 \leq y \leq 1\}$, in which the influence radius is set to 0.25 [m]. The interval field is constructed by using 2D B-spline basis functions of the second degree, illustrated in Fig.18. Note that the support of the basis functions, within which the partition of unity is fulfilled, must enclose the plate. Figure.19 displays two realisations of the interval field of Young's modulus.

Results are obtained from a total number of 10^5 Monte Carlo simulations. The crisp bounds of the

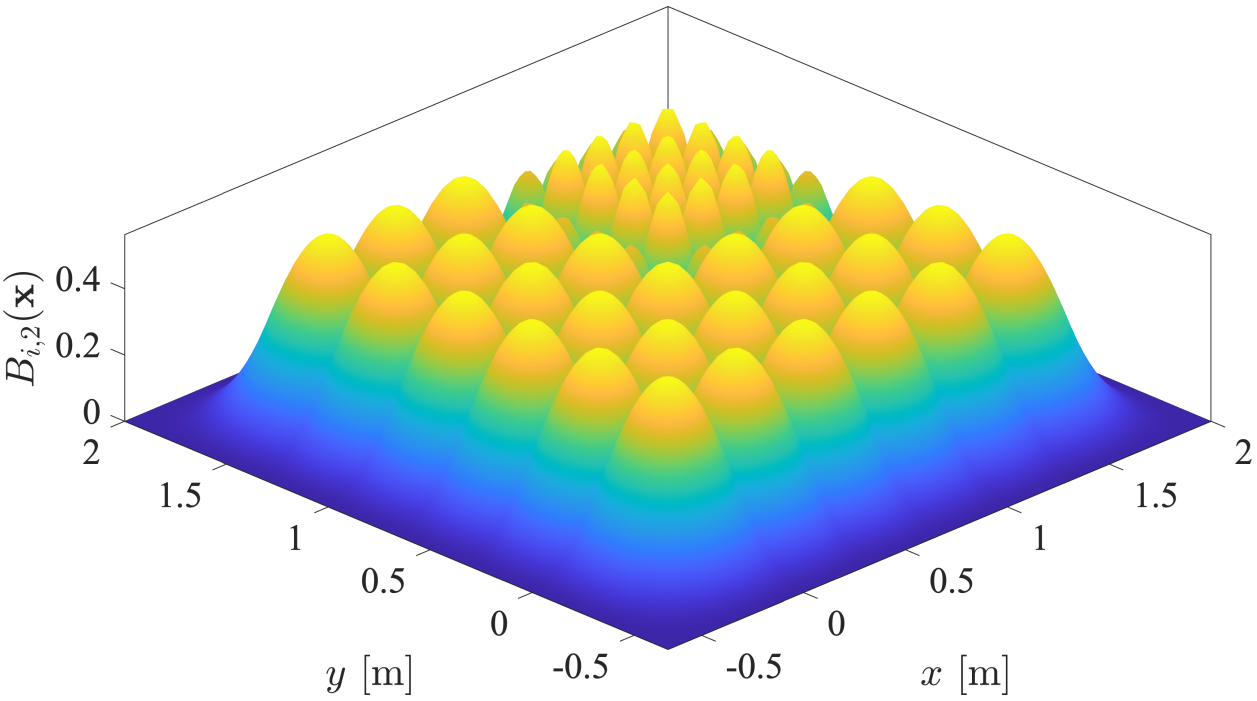

Fig. 18. Basis functions with 2 levels.

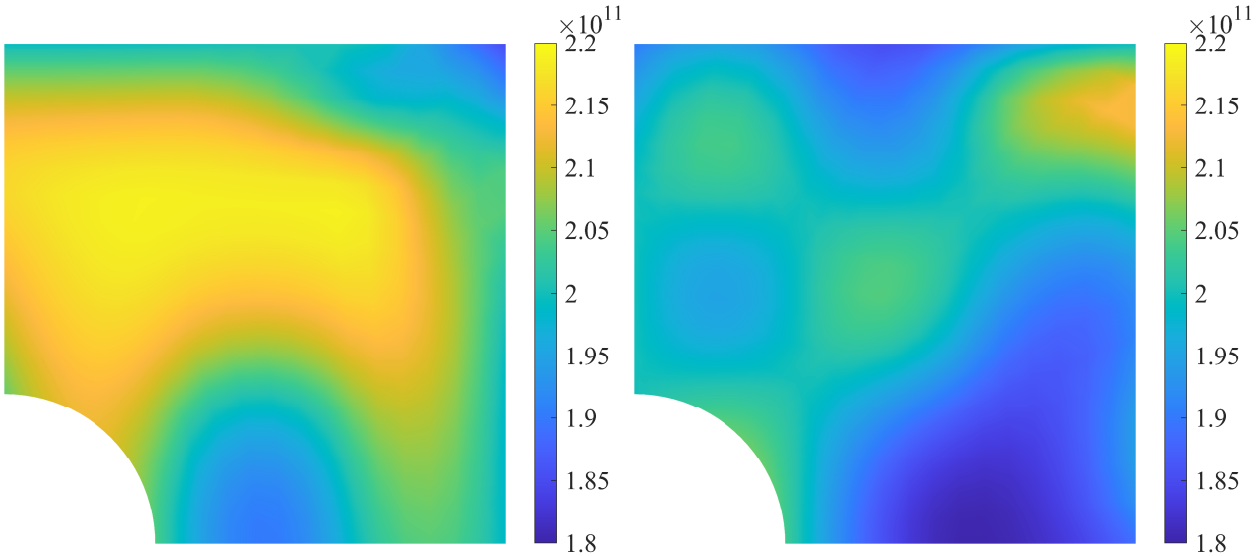

(a) **(b)**

Fig. 19. Two realisations of the distribution of Young's modulus. In [Pa].

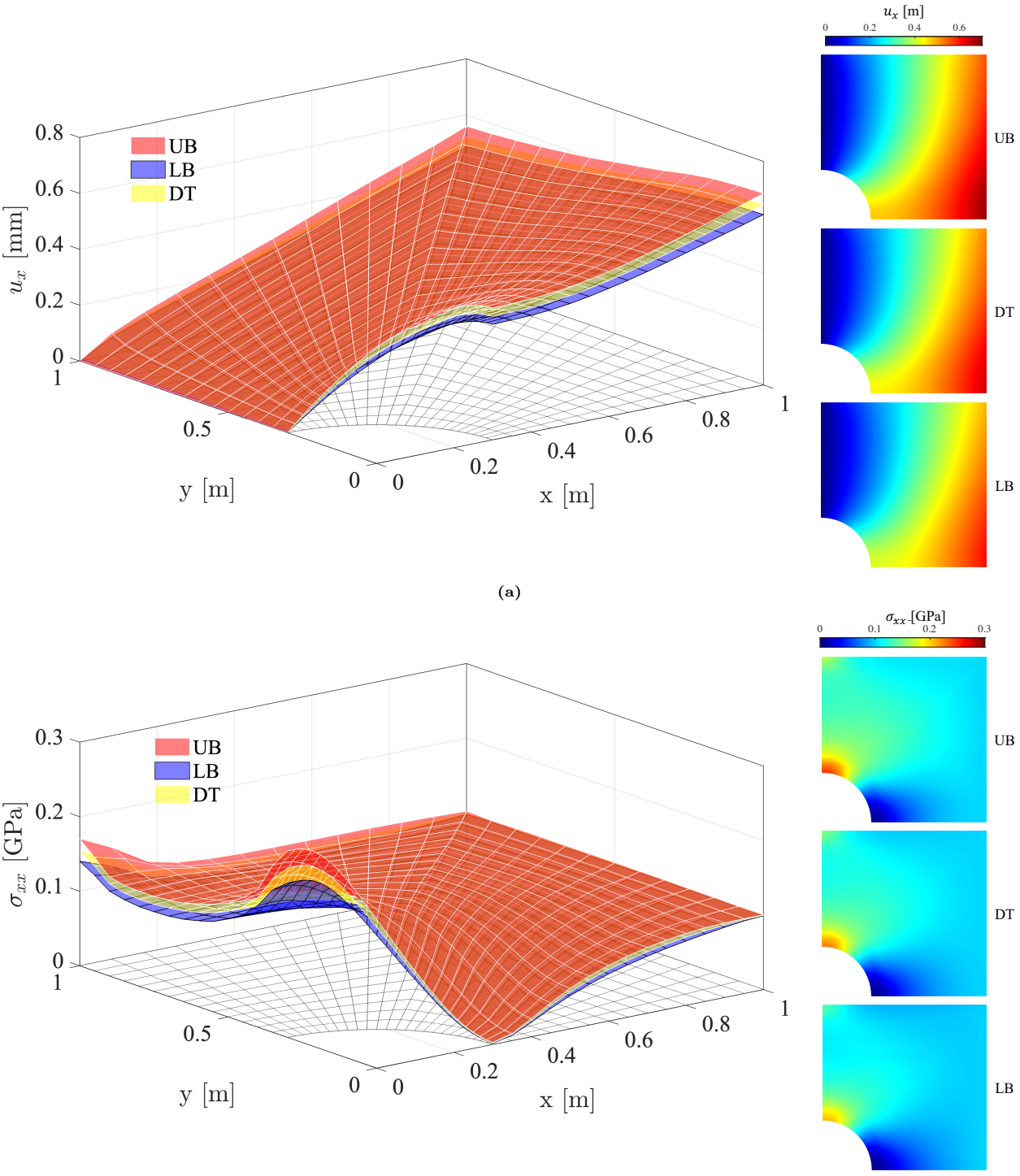

Fig. 20. (a) Displacements and (b) stress in the x-direction. UB/LB: upper and lower bounds of the outputs by the interval field model, DT: output of the deterministic model.

displacement and stress in the x-direction are shown in Fig.20. The deterministic results are also shown as a reference, computed by setting the interval radius to zero. It can be observed that both bounds of the interval field model enclose the deterministic results. Furthermore, the same number of simulations are also conducted to model Young's modulus of each point in the plate as an independent interval variable with bounds $[E_c - E_r, E_c + E_r]$. To compare the results from the interval field model (IF), independent interval model (II) and the deterministic model (DT), the displacement and stress in the x-direction of the points $(1, 0)$ is collected and shown in Table.3. It can be observed from the table that the results of the IF model have narrower bounds compared with those of the II model, which shows that the II model can be conservative when the cross dependency of the interval variables is taken into account and the IF model can be more suitable in such circumstances.

Table 3: Comparison of results at the point (1, 0).

Model	u_x [mm]	σ_{xx} [GPa]
DT	0.6466	0.0996
IF	$[0.6096, 0.6852]$	$[0.0989, 0.1003]$
II	$[0.5878, 0.7185]$	$[0.0962, 0.1030]$

6. Conclusions

A new explicit interval field formulation, termed B-spline based interval field decomposition (BIFD) method, is proposed in this paper to account for spatial dependencies among interval variables in the field. Using the partition of unity of the B-spline basis functions, an intuitive formulation directly constituted by interval properties is easily obtained. Moreover, the fast evaluation of B-spline functions alleviates the computational burden to a large extent, thus facilitating the use of the BIFD method in higher dimensional or more complex problems. The proposed BIFD method allows to take into account known values for the interval field at some locations and impose zero-interval at these locations. The interval field construction with such deterministic local values also addresses the variations of bounds effectively quantified through optimisation methods. The extension of the BIFD method for modelling inhomogeneous interval fields is performed. Two approaches, namely BIFD with truncated hierarchical B-spline (THB-spline) basis functions and multi-patch stitching method, are proposed to account for the local effects. These approaches succeed in modelling inhomogeneous interval fields. Finally, the numerical cases show that the BIFD method can generate reasonable output bounds while avoiding being too conservative, and taking into account local known values in the interval field can significantly reduce the output bounds and avoid over-consevartism.

Acknowledgments

The first author H. Hu gratefully acknowledges the financial support from the University of Liverpool and China Scholarship Council Awards (CSC NO.201906230311).

Appendix A Dependency function and dependency length of interval field with the BIFD method.

In the probabilistic framework, correlation length is used to characterise the distance within which two points in the field are considered to be correlated. It is generally defined as a parameter in the correlation function. For example, let x_1 and x_2 be two random variables in the field, the correlation function in the Gaussian form can be expressed as

$$\operatorname{corr}(x_1, x_2) = \frac{\mathbb{E}[(x_1 - \mu_{x_1})(x_2 - \mu_{x_2})]}{\sigma_{x_1}\sigma_{x_2}} = \mathrm{e}^{-\frac{\|x_1 - x_2\|^2}{l_c^2}}, \tag{A.1}$$

where $\mathbb{E}[\bullet]$ denotes the mathematical expectation and $\mu_x = \mathbb{E}[x]$, $\sigma_x = \sqrt{\mathbb{E}[(x-\mu_x)^2]}$ are the mean value and standard deviation, respectively. $\| \bullet \|$ denotes Euclidean norm and l_c denotes the correlation length. Analogously, define the operator $\langle \bullet \rangle$ to compute the interval centre for an interval scalar $x^{\mathrm{I}} \in [\underline{x}, \overline{x}]$ such as

$$\langle x^{\mathrm{I}} \rangle = (\underline{x} + \overline{x})/2. \tag{A.2}$$

Here the term 'dependency function' is used to quantify the dependencies between interval scalars and it is defined as

$$\operatorname{Dep}^{\mathrm{I}}(x_1^{\mathrm{I}}, x_2^{\mathrm{I}}) = \frac{\langle (x_1^{\mathrm{I}} - \langle x_1^{\mathrm{I}} \rangle)(x_2^{\mathrm{I}} - \langle x_2^{\mathrm{I}} \rangle) \rangle}{\sqrt{\langle (x_1^{\mathrm{I}} - \langle x_1^{\mathrm{I}} \rangle)^2 \rangle}\sqrt{\langle (x_2^{\mathrm{I}} - \langle x_2^{\mathrm{I}} \rangle)^2 \rangle}} = \frac{\langle x_1^{\mathrm{I}} x_2^{\mathrm{I}} \rangle - \langle x_1^{\mathrm{I}} \rangle \langle x_2^{\mathrm{I}} \rangle}{\sqrt{\langle x_1^{\mathrm{I}2} \rangle}\sqrt{\langle x_2^{\mathrm{I}2} \rangle}}. \tag{A.3}$$

For an interval field defined on domain Ω with influence radius R_d, a knot vector $\Xi = [t_1, t_2, \ldots, t_{N+k+1}]$ can be determined through Algorithm 1 such that $\Omega \subseteq [t_{k+1}, t_N]$, based on which a set of B-spline basis functions $\{B_{i,k}(x)\}_{i=1}^{N}$ of degree k can be determined. For the ease of notation we set the interval centre to zero ($H_c = 0$) and interval radius to one ($H_r = 1$), the interval field can thus be obtained as

$$\mathbb{H}^{\mathrm{I}}(x) = H_c + H_r \sum_{i=1}^{N} B_{i,k}(x)\, \xi_i^{\mathrm{I}}, \ x \in \Omega, \tag{A.4}$$

where $\{\xi_i^{\mathrm{I}}\}$ are independent unitary interval scalars. We define a dimensionless dependency function of two

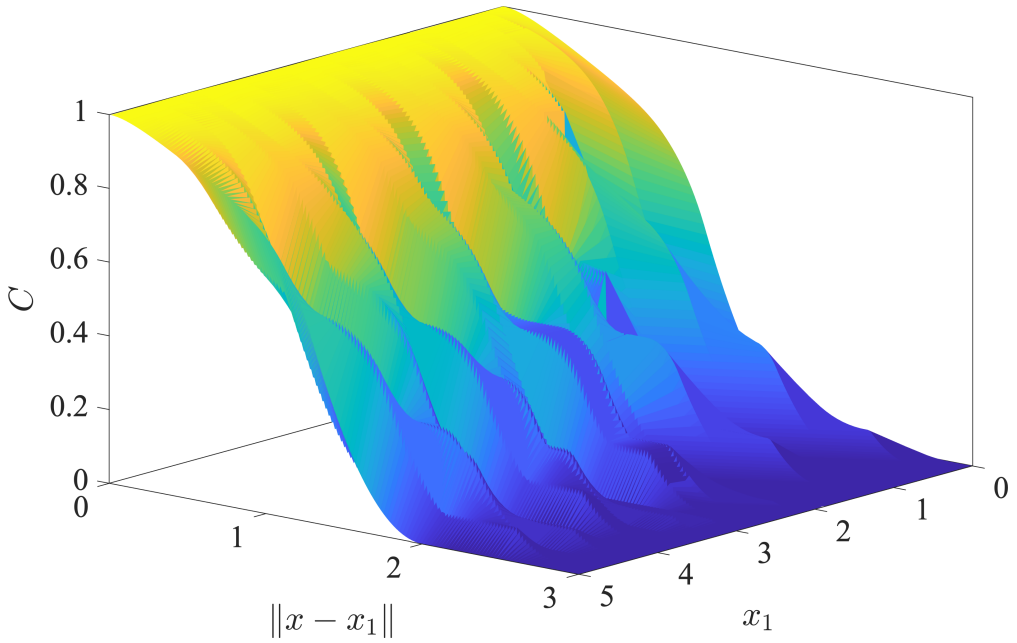

Fig. A.1. Evaluation of the dependency function with interval field parameters $\Omega = [0, 10],\ H_c = 0,\ H_r = 1,\ R_d = 1.5,\ k = 2$ and knot vector $\Xi = [-2, -1, 0, 1, 2, 3, 4, 5, 6, 7, 8, 9, 10, 11, 12]$.

points $x_1,\ x_2$ in the field to illustrate their spatial dependency as

$$
\begin{aligned}
C_{\mathbb{H}}(x_1, x_2) &= \mathrm{Dep}^{\mathrm{I}}(\mathbb{H}^{\mathrm{I}}(x_1), \mathbb{H}^{\mathrm{I}}(x_2)) \\
&= \frac{\langle \mathbb{H}^{\mathrm{I}}(x_1) \cdot \mathbb{H}^{\mathrm{I}}(x_2) \rangle - \langle \mathbb{H}^{\mathrm{I}}(x_1) \rangle \cdot \langle \mathbb{H}^{\mathrm{I}}(x_2) \rangle}{\sqrt{\langle \mathbb{H}^{\mathrm{I2}}(x_1) \rangle} \sqrt{\langle \mathbb{H}^{\mathrm{I2}}(x_2) \rangle}} \\
&= \max\{\sum_{i=1}^{N} B_{i,k}(x_1)\, \xi_i^{\mathrm{I}} \cdot \sum_{j=1}^{N} B_{j,k}(x_2)\, \xi_j^{\mathrm{I}}\} + \min\{\sum_{i=1}^{N} B_{i,k}(x_1)\, \xi_i^{\mathrm{I}} \cdot \sum_{j=1}^{N} B_{j,k}(x_2)\, \xi_j^{\mathrm{I}}\} \\
&= 1 + \min(\boldsymbol{\xi}^{\mathrm{T}} \mathbf{B}(x_1) \mathbf{B}^{\mathrm{T}}(x_2) \boldsymbol{\xi}),
\end{aligned}
\tag{A.5}
$$

where $\boldsymbol{\xi} = [\xi_1^{\mathrm{I}}, \xi_2^{\mathrm{I}}, \ldots, \xi_N^{\mathrm{I}}]^{\mathrm{T}}$ and $\mathbf{B}(x) = [B_{1,k}(x), B_{2,k}(x), \ldots, B_{N,k}(x)]^{\mathrm{T}}$.. The authors note that the determination of the dependency function becomes an optimisation problem as shown in the last equation of (A.5). Figure A.1 presents the results of the evaluation of dependency function of the interval field with field parameters indicated in the caption of the figure. It is clearly observed that the field is non-stationary as the dependency coefficient varies when x_1 takes distinct positions in the field, especially when x_1 is coincident with the knot. This is because the total span of B-spline basis functions that contains a knot point is always smaller than the total span of those basis functions containing a non-knot point, which makes the knot point slightly less 'influential' in the field.

Practically, the dependency structure of the interval field can be quantified through numerical realisations. Discretise the domain Ω and take M increasing coordinates $[\hat{x}_1, \hat{x}_2, \ldots, \hat{x}_M]$ such that $\hat{x}_{i+m} = \hat{x}_i + m\tau,\ 1 \leq$

$i \leq M-1,\ 1 \leq m \leq M-i$. Following [33], define the dependency function as

$$C^{\mathrm{I}}_{\mathbb{H}}(m\tau) = C_{\mathbb{H}}(\hat{x}_i, \hat{x}_{i+m}) = \frac{\langle \mathbb{H}^{\mathrm{I}}(\hat{x}_i) \cdot \mathbb{H}^{\mathrm{I}}(\hat{x}_{i+m})\rangle - \langle \mathbb{H}^{\mathrm{I}}(\hat{x}_i)\rangle \cdot \langle \mathbb{H}^{\mathrm{I}}(\hat{x}_{i+m})\rangle}{\sqrt{\langle \mathbb{H}^{\mathrm{I2}}(\hat{x}_i)\rangle}\sqrt{\langle \mathbb{H}^{\mathrm{I2}}(\hat{x}_{i+m})\rangle}}$$
$$= \max_{i=1,\ldots,M-m}\{\mathbb{H}^{\mathrm{I}}(\hat{x}_i) \cdot \mathbb{H}^{\mathrm{I}}(\hat{x}_i + m\tau\} + \min_{i=1,\ldots,M-m}\{\mathbb{H}^{\mathrm{I}}(\hat{x}_i) \cdot \mathbb{H}^{\mathrm{I}}(\hat{x}_i + m\tau)\},\ m = 1, 2, \ldots, M-1. \tag{A.6}$$

The dependency function is then modified in the following way to maintain a decreasing trend of the depen-

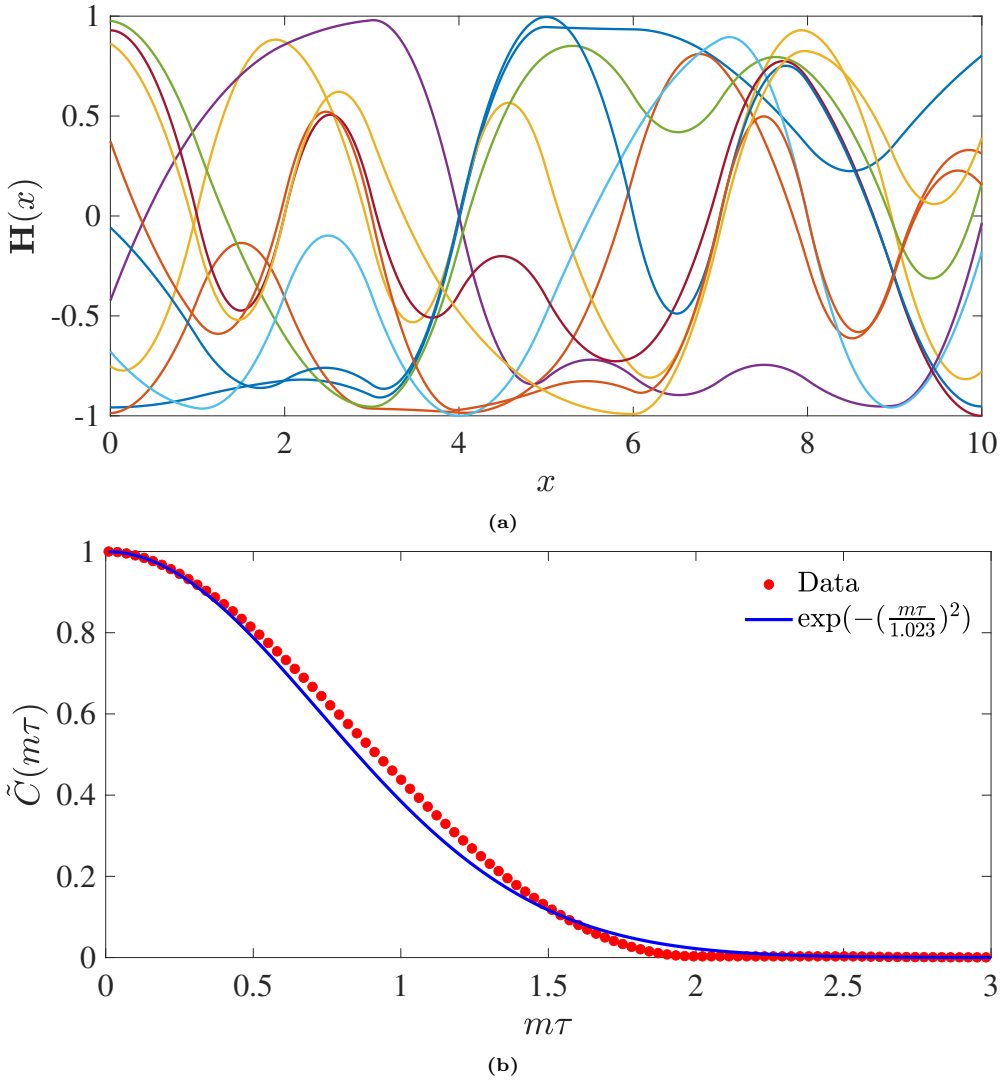

Fig. A.2. (a) Ten realisations of the interval field with the same field parameters as shown in Fig.A.1; (b) dependency coefficients and the curve fitting into the Gaussian form.

dency coefficient in an increasing distance between measured points and also to ensure the non-negativity of the dependency coefficient as

$$\tilde{C}^{\mathrm{I}}_{\mathbb{H}}(m\tau) = \max\{0, \min\{C^{\mathrm{I}}_{\mathbb{H}}(\tau), C^{\mathrm{I}}_{\mathbb{H}}(2\tau), \ldots, C^{\mathrm{I}}_{\mathbb{H}}(m\tau)\}\},\ m = 1, 2, \ldots, M-1. \tag{A.7}$$

Figure A.2(a) illustrates ten realisations of the interval field, based on which the dependency coefficients

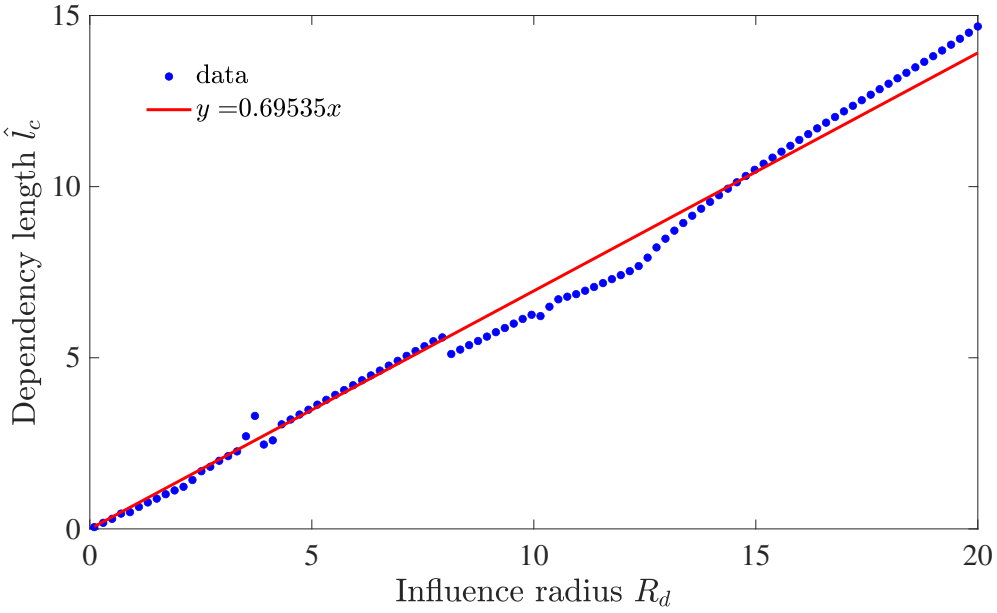

Fig. A.3. Approximately linear relationship between influence radius and dependency length.

are calculated by (A.6) and (A.7) and are shown in Fig.A.2(b) with respect to $m\tau$. These data are then interpolated with least square fitting technique into the exponential form as shown in (A.1) to identify the corresponding dependency length. The result reveals that the dependency structure of the interval field realisations is consistent with the dependency function of the exponential form with a dependency length identified as $\hat{l}_c = 1.023$.

A further analysis is performed to see whether the influence radius and the corresponding dependency length have a stable relation. Multiple realisations of the interval field with varying influence radii are conducted. For each case, the corresponding dependency length of the exponential form is identified by least-squares fitting technique. The results are depicted in Fig.A.3 and are interpolated by a linear function. It is observed that a linear relationship between the influence radius and the estimated dependency length is approximately satisfied as

$$\hat{l}_c \approx 0.69535\, R_d. \tag{A.8}$$

Such an approximately linear relation demonstrates that the influence radius of the interval field plays the role of the correlation length in the probabilistic framework, with the only difference of a scaling factor.

The dependency structure of a multi-dimensional interval field is beyond the scope of this paper but it is an interesting research topic worth investigating in the future.

Appendix B Interval finite element formulation

A typical linear FEM problem is built upon the domain of interest $\mathcal{A}$ that is discretised by several finite elements, e.g. $\mathcal{A} = \bigcup_{i\in I} \mathcal{A}_i$ where I is the set of all element indices. The equilibrium equation of an element can be constructed as

$$\mathbf{K}_\mathrm{e}\mathbf{u}_\mathrm{e} = \mathbf{F}_\mathrm{e}, \tag{B.1}$$

where $\mathbf{u}_\mathrm{e}$ is the element-based vector of nodal displacements, $\mathbf{F}_\mathrm{e}$ is the element-based vector of equivalent nodal forces. $\mathbf{K}_\mathrm{e}$ is the element stiffness matrix that has the form of

$$\mathbf{K}_\mathrm{e} = \int_{\mathcal{A}_\mathrm{e}} \mathbf{B}^\mathrm{T}\mathbf{D}\mathbf{B}\mathrm{d}\mathcal{A}, \tag{B.2}$$

where $\mathbf{B}$ is the strain-displacement matrix and $\mathbf{D}$ is the elasticity matrix comprised of material parameters such as Young's modulus E and Poisson's ratio ν. In the non-deterministic setting, the uncertainties in the material properties can be taken into account and thus making $\mathbf{D}$ a non-deterministic matrix. For instance, an interval field modelling of Young's modulus of an interval centre E_c, interval radius E_r and influence radius R_d has the form of

$$\mathbb{E}^\mathrm{I}(\mathbf{x}) = E_c + E_r \sum_i B_{i,2}(\mathbf{x})\,\xi_i^\mathrm{I},\ \mathbf{x}\in\mathcal{A}, \tag{B.3}$$

where $\mathbb{E}^\mathrm{I}(\mathbf{x})$ is expanded by second order B-splines basis functions that have support in $\mathcal{A}$ and are controlled by the influence radius, and $\{\xi_i^\mathrm{I}\}$ are IFCs. In such a case, the elasticity matrix becomes an interval matrix and so is the element stiffness matrix, which can be expressed as

$$\mathbf{K}_\mathrm{e}^\mathrm{I}(\mathbf{x},\boldsymbol{\xi}^\mathrm{I}) = \int_{\mathcal{A}_\mathrm{e}} \mathbf{B}^\mathrm{T}\mathbf{D}^\mathrm{I}(\mathbf{x},\boldsymbol{\xi}^\mathrm{I})\mathbf{B}\mathrm{d}\mathcal{A}, \tag{B.4}$$

where $\boldsymbol{\xi}^\mathrm{I} = \{\xi_i^\mathrm{I}\}$. Finally, the global stiffness matrix and force vector can be obtained as

$$\mathbf{K}^\mathrm{I}(\mathbf{x},\boldsymbol{\xi}) = \mathop{\mathrm{A}}_{e=1}^{n_e} \mathbf{K}_\mathrm{e}(\mathbf{x},\boldsymbol{\xi}^\mathrm{I}),\ \mathbf{F} = \mathop{\mathrm{A}}_{e=1}^{n_e} \mathbf{F}_\mathrm{e}, \tag{B.5}$$

where $\mathop{\mathrm{A}}$ denotes the standard finite element assembly procedure. The equilibrium equation for the system can thus be expressed as

$$\mathbf{K}^\mathrm{I}(\mathbf{x},\boldsymbol{\xi})\mathbf{u} = \mathbf{F}. \tag{B.6}$$

Note that due to the interval matrix $\mathbf{K}^\mathrm{I}(\mathbf{x},\boldsymbol{\xi})$ the displacement vector to be sought also becomes an interval vector, e.g. $\mathbf{u} = \mathbf{u}^\mathrm{I}(\mathbf{x},\boldsymbol{\xi})$. In most cases, solving (B.6) directly can be much complicated. Instead, the solution of interest is usually to estimate its upper and lower bounds through numerical methods such as

Monte Carlo method or (anti-) optimisation methods. In this paper, Monte Carlo method is adopted.

References

[1] G. CHRISTAKOS, 2 - the spatial random field model, in: G. CHRISTAKOS (Ed.), Random Field Models in Earth Sciences, Academic Press, Boston, 1992, pp. 21–106. doi:https://doi.org/10.1016/B978-0-12-174230-0.50007-X.

[2] H. Hu, A. Batou, H. Ouyang, Coefficient of friction random field modelling and analysis in planar sliding, Journal of Sound and Vibration 508 (2021) 116197. doi:https://doi.org/10.1016/j.jsv.2021.116197.

[3] R. G. Ghanem, P. D. Spanos, Stochastic finite elements: a spectral approach, Courier Corporation, 2003. doi:https://doi.org/10.1007/978-1-4612-3094-6.

[4] R. E. Moore, R. B. Kearfott, M. J. Cloud, Introduction to interval analysis, SIAM, 2009. doi:10.1137/1.9780898717716.ch1.

[5] L. Jaulin, M. Kieffer, O. Didrit, E. Walter, Interval analysis, in: Applied interval analysis, Springer, 2001, pp. 11–43. doi:https://doi.org/10.1007/978-1-4471-0249-6.

[6] H.-J. Zimmermann, Fuzzy set theory—and its applications, Springer Science & Business Media, 2011. doi:https://doi.org/10.1007/978-94-015-7949-0.

[7] H. Zimmermann, Fuzzy Set Theory—and Its Applications, Springer Netherlands, 2001. doi:https://doi.org/10.1007/978-94-010-0646-0.

[8] G. Shafer, A mathematical theory of evidence, Princeton university press, 1976. doi:https://doi.org/10.1515/9780691214696.

[9] J. A. Barnett, Computational methods for a mathematical theory of evidence, in: Classic Works of the Dempster-Shafer Theory of Belief Functions, Springer, 2008, pp. 197–216. doi:https://doi.org/10.1007/978-3-540-44792-4_8.

[10] M. Beer, S. Ferson, V. Kreinovich, Imprecise probabilities in engineering analyses, Mechanical systems and signal processing 37 (1-2) (2013) 4–29. doi:https://doi.org/10.1016/j.ymssp.2013.01.024.

[11] T. Augustin, F. P. Coolen, G. De Cooman, M. C. Troffaes, Introduction to imprecise probabilities, John Wiley & Sons, 2014. doi:10.1002/9781118763117.

[12] R. Kang, Q. Zhang, Z. Zeng, E. Zio, X. Li, Measuring reliability under epistemic uncertainty: Review on non-probabilistic reliability metrics, Chinese Journal of Aeronautics 29 (3) (2016) 571–579. doi:https://doi.org/10.1016/j.cja.2016.04.004.

[13] M. Faes, D. Moens, Recent trends in the modeling and quantification of non-probabilistic uncertainty, Archives of Computational Methods in Engineering 27 (3) (2020) 633–671. doi:https://doi.org/10.1007/s11831-019-09327-x.

[14] S. Guo, Z. Lu, Interval arithmetic and static interval finite element method, APPLIED MATHEMATICS AND MECHANICS-ENGLISH EDITION 22 (12) (2001) 1390–1396. doi:{10.1023/A:1022826525318}.

[15] S.-H. Chen, X.-W. Yang, Interval finite element method for beam structures, Finite elements in analysis and design 34 (1) (2000) 75–88. doi:https://doi.org/10.1016/S0168-874X(99)00029-3.

[16] D. Moens, M. De Munck, W. Desmet, D. Vandepitte, Numerical dynamic analysis of uncertain mechanical structures based on interval fields, in: IUTAM symposium on the vibration analysis of structures with uncertainties, Springer, 2011, pp. 71–83. doi:https://doi.org/10.1007/978-94-007-0289-9_6.

[17] M. Faes, M. Imholz, D. Vandepitte, D. Moens, A review of interval field approaches for uncertainty quantification in numerical models, Modern Trends in Structural and Solid Mechanics 3: Non-deterministic Mechanics (2021) 95–110doi:https://doi.org/10.1002/9781119831839.ch6.

[18] M. Faes, Interval methods for the identification and quantification of inhomogeneous uncertainty in finite element models, Ph.D. thesis (11 2017).

[19] M. Faes, D. Moens, Identification and quantification of spatial interval uncertainty in numerical models, Computers & Structures 192 (2017) 16–33. doi:https://doi.org/10.1016/j.compstruc.2017.07.006.

[20] C. van Mierlo, M. G. Faes, D. Moens, Inhomogeneous interval fields based on scaled inverse distance weighting interpolation, Computer Methods in Applied Mechanics and Engineering 373 (2021) 113542. doi:https://doi.org/10.1016/j.cma.2020.113542.

[21] R. R. Callens, M. G. Faes, D. Moens, Local explicit interval fields for non-stationary uncertainty modelling in finite element models, Computer Methods in Applied Mechanics and Engineering 379 (2021) 113735. doi:https://doi.org/10.1016/j.cma.2021.113735.

[22] M. Imholz, D. Vandepitte, D. Moens, Derivation of an input interval field decomposition based on expert knowledge using locally defined basis functions, in: UNCECOMP 2015-1st ECCOMAS Thematic Conference on Uncertainty Quantification in Computational Sciences and Engineering, 2015, pp. 529–547. doi:https://doi.org/10.7712/120215.4290.583.

[23] M. Imholz, D. Vandepitte, D. Moens, Analysis of the effect of uncertain clamping stiffness on the dynamical behaviour of structures using interval field methods, in: Applied mechanics and materials, Vol. 807, Trans Tech Publ, 2015, pp. 195–204. doi:https://doi.org/10.4028/www.scientific.net/AMM.807.195.

[24] Z.-Y. Chen, M. Imholz, L. Li, M. Faes, D. Moens, Transient landing dynamics analysis for a lunar lander with random and interval fields, Applied Mathematical Modelling 88 (2020) 827–851. doi:https://doi.org/10.1016/j.apm.2020.06.075.

[25] A. Sofi, Structural response variability under spatially dependent uncertainty: stochastic versus interval model, Probabilistic Engineering Mechanics 42 (2015) 78–86. doi:https://doi.org/10.1016/j.probengmech.2015.09.001.

[26] A. Sofi, Euler-Bernoulli interval finite element with spatially varying uncertain properties, Acta Mechanica 228 (11) (2017) 3771–3787. doi:https://doi.org/10.1007/s00707-017-1903-7.

[27] A. Sofi, G. Muscolino, I. Elishakoff, Static response bounds of timoshenko beams with spatially varying interval uncertainties, Acta Mechanica 226 (11) (2015) 3737–3748. doi:https://doi.org/10.1007/s00707-015-1400-9.

[28] A. Sofi, E. Romeo, O. Barrera, A. Cocks, An interval finite element method for the analysis of structures with spatially varying uncertainties, Advances in Engineering Software 128 (2019) 1–19. doi:https://doi.org/10.1016/j.advengsoft.2018.11.001.

[29] C. Jiang, B. Ni, X. Han, Y. Tao, Non-probabilistic convex model process: a new method of time-variant uncertainty analysis and its application to structural dynamic reliability problems, Computer Methods in Applied Mechanics and Engineering 268 (2014) 656–676. doi:https://doi.org/10.1016/j.cma.2013.10.016.

[30] J. Li, B. Ni, C. Jiang, T. Fang, Dynamic response bound analysis for elastic beams under uncertain excitations, Journal of Sound and Vibration 422 (2018) 471–489. doi:https://doi.org/10.1016/j.jsv.2018.02.025.

[31] C. Jiang, B. Ni, N. Liu, X. Han, J. Liu, Interval process model and non-random vibration analysis, Journal of Sound and Vibration 373 (2016) 104–131. doi:https://doi.org/10.1016/j.jsv.2016.03.019.

[32] B. Ni, C. Jiang, Interval field model and interval finite element analysis, Computer Methods in Applied Mechanics and Engineering 360 (2020) 112713. doi:https://doi.org/10.1016/j.cma.2019.112713.

[33] Y. Luo, J. Zhan, J. Xing, Z. Kang, Non-probabilistic uncertainty quantification and response analysis of structures with a bounded field model, Computer Methods in Applied Mechanics and Engineering 347 (2019) 663–678. doi:https://doi.org/10.1016/j.cma.2018.12.043.

[34] J. Zhan, Y. Luo, X. Zhang, Z. Kang, A general assessment index for non-probabilistic reliability of structures with bounded field and parametric uncertainties, Computer Methods in Applied Mechanics and Engineering 366 (2020) 113046. doi:https://doi.org/10.1016/j.cma.2020.113046.

[35] R. L. Muhanna, R. L. Mullen, Uncertainty in mechanics problems—interval–based approach, Journal of Engineering Mechanics 127 (6) (2001) 557–566. doi:10.1061/(ASCE)0733-9399(2001)127:6(557).

[36] A. Sofi, E. Romeo, A novel interval finite element method based on the improved interval analysis, Computer Methods in Applied Mechanics and Engineering 311 (2016) 671–697. doi:https://doi.org/10.1016/j.cma.2016.09.009.

[37] L. Piegl, W. Tiller, The NURBS book, Springer Science & Business Media, 1996. doi:https://doi.org/10.1007/978-3-642-59223-2.

[38] M. Faes, J. Cerneels, D. Vandepitte, D. Moens, Identification and quantification of multivariate interval uncertainty in finite element models, Computer Methods in applied mechanics and engineering 315 (2017) 896–920. doi:https://doi.org/10.1016/j.cma.2016.11.023.

[39] P. Boggs, J. Tolle, Sequential quadratic programming, Acta Numerica 4 (1995) 1–51. doi:10.1017/S0962492900002518.

[40] H. Maatouk, X. Bay, Gaussian process emulators for computer experiments with inequality constraints, Mathematical Geosciences 49 (2017) 557–582. doi:https://doi.org/10.1007/s11004-017-9673-2.

[41] N. D. Lawrence, Gpmat, https://github.com/SheffieldML/GPmat (2015).

[42] D. R. Forsey, R. H. Bartels, Hierarchical b-spline refinement, in: Proceedings of the 15th annual conference on Computer graphics and interactive techniques, 1988, pp. 205–212. doi:https://doi.org/10.1145/54852.378512.

[43] C. Giannelli, B. Jüttler, H. Speleers, THB-splines: The truncated basis for hierarchical splines, Comput. Aided Geom. Des. 29 (2012) 485–498. doi:https://doi.org/10.1016/j.cagd.2012.03.025.

[44] A. W. Leissa, M. S. Qatu, Vibrations of continuous systems, McGraw-Hill Education, 2011. URL https://www.accessengineeringlibrary.com/content/book/9780071714792